Seasonal cycle of $C^{16}O^{16}O$, $C^{16}O^{17}O$, and $C^{16}O^{18}O$ in the middle atmosphere: Implications for mesospheric dynamics and biogeochemical sources and sinks of CO_2

Mao-Chang Liang,[1,2,3] Geoffrey A. Blake,[3] and Yuk L. Yung[3]

Received 3 January 2007; revised 24 November 2007; accepted 17 December 2008; published 21 June 2008.

[1] The isotopic anomaly of oxygen in atmospheric CO_2 is caused by exchange reactions with isotopically anomalous $O(^1D)$ in the middle atmosphere. In the stratosphere, the major source of $O(^1D)$ is O_3 photolysis; O_3 is known to possess mass-independent isotopic composition, with $\delta^{49}O_3 \approx \delta^{50}O_3 \approx 100‰$ relative to atmospheric O_2. Higher in the mesosphere, Lyman α-driven photodissociation of O_2 provides a more important source of heavy $O(^1D)$ than O_3 photolysis. Here we present a two-dimensional simulation of the isotopic composition of CO_2 from the surface to an altitude of $\sim$130 km that adequately reproduce the observed seasonal cycle of CO_2 in the upper troposphere and the age of air in the stratosphere. Our model results suggest that stratospheric-tropospheric exchange not only modifies the level of heavy CO_2 in the troposphere, but also influences its seasonal cycle. Thus the isotopic composition of CO_2 in the troposphere/biosphere could be affected by the downwelling air from the stratosphere. The predicted size of the effect is detectable by current instrumentation. Implications for the use of the isotopic composition of CO_2 to constrain the gross carbon flux between the atmosphere and terrestrial biosphere and the dynamics in the remote mesosphere are discussed.

Citation: Liang, M.-C., G. A. Blake, and Y. L. Yung (2008), Seasonal cycle of $C^{16}O^{16}O$, $C^{16}O^{17}O$, and $C^{16}O^{18}O$ in the middle atmosphere: Implications for mesospheric dynamics and biogeochemical sources and sinks of CO_2, *J. Geophys. Res.*, *113*, D12305, doi:10.1029/2007JD008392.

1. Introduction

[2] Carbon dioxide is an important greenhouse gas, yet the understanding of its sources and sinks is far from satisfactory. The major difficulty is caused by high CO_2 two-way fluxes between the atmosphere and planetary surface, resulting in a large seasonality of the CO_2 mixing ratio at the surface. For example, as reported by *IPCC* [2001], the flux of CO_2 between the atmosphere and the surface is $\sim$200 PgC/a, and the ''net'' uptake on the surface is $\sim$3 PgC/a. A measurement accuracy of better than 1%, or CO_2 mixing ratios <3 parts per million by volume (ppmv), is therefore required to quantify the sources and sinks of CO_2. While in situ techniques [e.g., *Tans et al.*, 1998; *GLOBALVIEW-CO_2*, 2007] have high accuracy, they possess limited spatial coverage. Satellite measurements provide much better spatial coverage but with lower precision [*Buchwitz et al.*, 2005a, 2005b]. Next generation satellites designed specifically to measure atmospheric CO_2, such as the Orbiting Carbon Observatory [*Kuang et al.*, 2002; *Crisp et al.*, 2004], will return column-averaged CO_2 mixing ratios under clear conditions with a precision of 1 ppmv.

[3] The discovery of mass-independent oxygen isotopic fractionation (MIF) in middle atmospheric CO_2 [*Zipf and Erdman*, 1994; *Thiemens et al.*, 1995; *Thiemens*, 1999, 2006; *Alexander et al.*, 2001; *Lämmerzahl et al.*, 2002; *Boering et al.*, 2004] provides another opportunity to study the sources and sinks of surface CO_2 [*Hoag et al.*, 2005]. Because the known sources and sinks of surface CO_2 are mass-dependent [e.g., see *Luz and Barkan*, 2005; *Thiemens*, 2006] and because the MIF originates in the middle atmosphere, isotopic measurements of atmospheric CO_2 can therefore be used to trace the biogeochemistry of carbon dioxide. Higher in the upper stratosphere and mesosphere, the isotopic composition of CO_2 (see below) provides a unique tool for studying atmospheric transport and chemistry because of its high abundance ($\sim$370 ppmv in the stratosphere, dropping to $\sim$100 ppmv at 100 km); the concentrations of other common tracers (e.g., CH_4, N_2O, SF_6, and the CFCs) are too low to be detected in the mesosphere. The MIF of CO_2 is caused by isotopic exchange reactions with $O(^1D)$ [*Thiemens et al.*, 1991; *Yung et al.*, 1991, 1997; *Liang et al.*, 2007], which is readily produced by the photolysis of O_3. The latter is known to be enriched in heavy isotopologues and isotopomers with highly nonmass dependent signatures [*Thiemens and Heidenreich*, 1983; *Mauersberger*, 1987; *Mauersberger et al.*, 1999, 2001; *Thiemens*, 2006].

[1]Research Center for Environmental Changes, Academia Sinica, Taipei, Taiwan.
[2]Graduate Institute of Astronomy, National Central University, Jongli, Taiwan.
[3]Division of Geological and Planetary Sciences, California Institute of Technology, Pasadena, California, USA.

0148-0227/08/2007JD008392

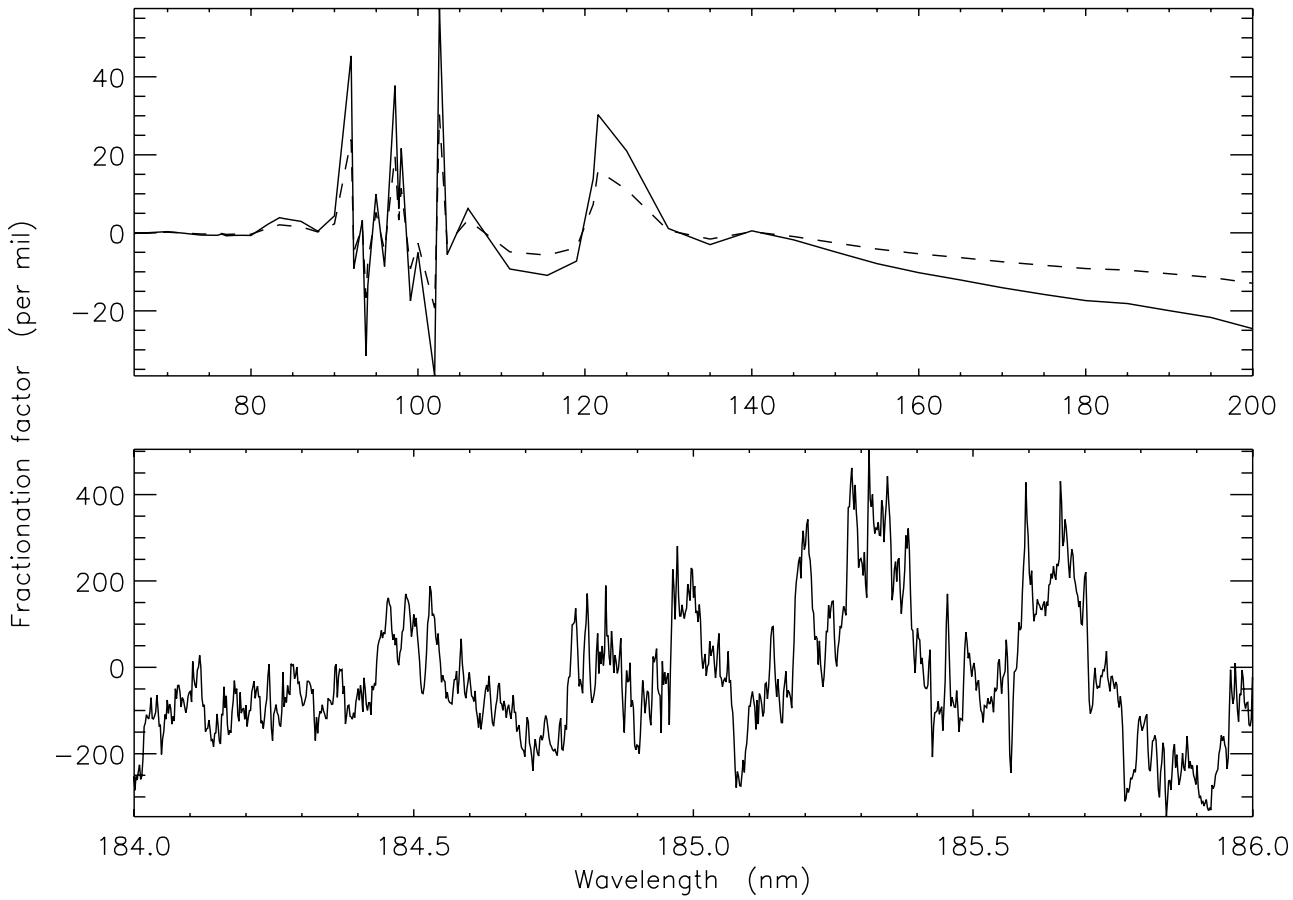

Figure 1. Photolytic fractionation factors of $C^{16}O^{18}O$ (solid) and $C^{16}O^{17}O$ (dashed), predicted with the method developed by *Yung and Miller* [1997]. The fractionation factor is defined by $\sigma/\sigma_0 - 1$, where σ and σ_0 are the photoabsorption cross sections of $C^{16}O^{18}O$ (and $C^{16}O^{17}O$) and $C^{16}O^{16}O$, respectively. The cross sections of normal CO_2 are taken from the literature [*Nakata et al.*, 1965; *Shemansky*, 1972; *Lawrence*, 1972a, 1972b; *Slanger and Black*, 1978; *Okabe*, 1978; *Hitchcock et al.*, 1980; *Lewis and Carver*, 1983; *Yoshino et al.*, 1996; *Parkinson et al.*, 2003]. For comparison with the experiments by *Bhattacharya et al.* [2000], high spectral resolution predictions for $C^{16}O^{18}O$ are shown in the lower panel. Detailed comparison requires the spectral function of the UV source used in the measurements. See, e.g., *Liang et al.* [2004] for details.

[4] The isotopic composition of atmospheric O_3 can be explained by two processes [*Liang et al.*, 2006] formation [*Thiemens and Heidenreich*, 1983; *Mauersberger et al.*, 1999; *Gao and Marcus*, 2001] and photolysis [*Blake et al.*, 2003; *Liang et al.*, 2004; *Miller et al.*, 2005]. The formation process results in $\delta^{49}O_3 \approx \delta^{50}O_3 \approx 100‰$, relative to atmospheric O_2, where ‰ denotes per mil or parts per thousand. About 10% of the observed O_3 isotopic enrichment in the stratosphere is due to photolytic processes, which provide an explanation for the observed altitude variation of the O_3 isotopic composition in the stratosphere. See *Liang et al.* [2006] for details. Initial photolysis experiments on O_3 suggested mass-independent isotopic fractionation [*Chakraborty and Bhattacharya*, 2003], but a reanalysis [*Cole and Boering*, 2006] of the available data shows that the measured laboratory isotopic compositions can be attributed solely to the formation of O_3. Thus no mass independent component is observed in the photolysis of O_3.

[5] Oxygen isotopic compositions are reported as $\delta^{17}O$ and $\delta^{18}O$. To be consistent with previous work [*Miller et al.*, 2005; *Liang et al.*, 2006, 2007; *Liang and Yung*, 2007], we define them here as

$$\delta^{17}O(CO_2) = \frac{[C^{16}O^{17}O]/[C^{16}O^{16}O]}{[^{16}O^{17}O]/[^{16}O^{16}O]} - 1 \quad (1)$$

$$\delta^{18}O(CO_2) = \frac{[C^{16}O^{18}O]/[C^{16}O^{16}O]}{[^{16}O^{18}O]/[^{16}O^{16}O]} - 1. \quad (2)$$

[6] Unless otherwise stated, the δ values reported in this paper are referenced to atmospheric O_2, rather than Vienna Standard Mean Ocean Water (V-SMOW). The magnitudes of atmospheric $\delta^{17}O(O_2)$ and $\delta^{18}O(O_2)$ are 11.75 and 23.5 ‰ referenced to V-SMOW [*Thiemens et al.*, 1995], respectively, while the values are zero as referenced to O_2 itself. A strictly mass-dependent isotopic composition follows

$$\delta^{17}O \approx 0.515\ \delta^{18}O, \quad (3)$$

Table 1. Two-Dimensional Chemical Transport Models[a]

	K_{yy}	K_{zz}	ψ	Altitude
Model A	Morgan et al.	Morgan et al.	Morgan et al.	0–80 km
Model B	Summers et al.	Summers et al.	WACCM	0–130 km
Model C	Morgan et al.	Morgan et al.	ECMWF	0–50 km
Model D	Morgan et al.	Morgan et al.	NCEP2	0–35 km
Model E	Morgan et al.	Morgan et al.	WACCM	0–80 km

[a]Morgan et al. and Summers et al. refer to *Morgan et al.* [2004] and *Summers et al.* [1997], respectively.

and the oxygen anomaly in this paper is defined as the residual from equation (3), or

$$\Delta^{17}O = \delta^{17}O - 0.515\ \delta^{18}O. \quad (4)$$

[7] In previous work, we have shown that two-dimensional (2-D) (latitude and height) models driven by the residual circulations derived from three-dimensional (3-D) (latitude, longitude, and height) wind fields can satisfactorily reproduce the age of air in the stratosphere [*Morgan et al.*, 2004] and the seasonality of CO_2 in the upper troposphere [*Shia et al.*, 2006]. Here, we adopt the same model as that described by *Shia et al.* [2006] and extend it to include other CO_2 isotopologues. This paper also represents an extension of the one-dimensional (1-D) (altitude) simulation of CO_2 isotopologues in the middle atmosphere by *Liang et al.* [2007], and is organized as follows. We briefly summarize the current view of the sources and sinks of CO_2 isotopologues in section 2. The chemistry of the MIF processes affecting CO_2 are described in section 3. The 2-D model is presented in section 4, followed by model results in section 5. A discussion of the results and the implications of the model results for the current and paleobiogeochemical cycles of CO_2 are presented in section 6.

2. Sources and Sinks of CO_2 Isotopologues

[8] Before the Industrial Era, the atmospheric CO_2 concentration was ~280 ppmv. It has been rising continuously since, reaching ~375 ppmv in 2004. The present atmospheric CO_2 increase is caused by anthropogenic emissions of CO_2. About three-quarters of the emissions are due to fossil fuel burning, ~5.4 ± 0.3 PgC/a during 1980–1989 and 6.3 ± 0.4 PgC/a over 1990–1999. Land use is largely responsible for the remainder. Not all the emitted CO_2 remains in the atmosphere. The uptake of CO_2 by land and ocean reduces the rate of CO_2 atmospheric accumula-

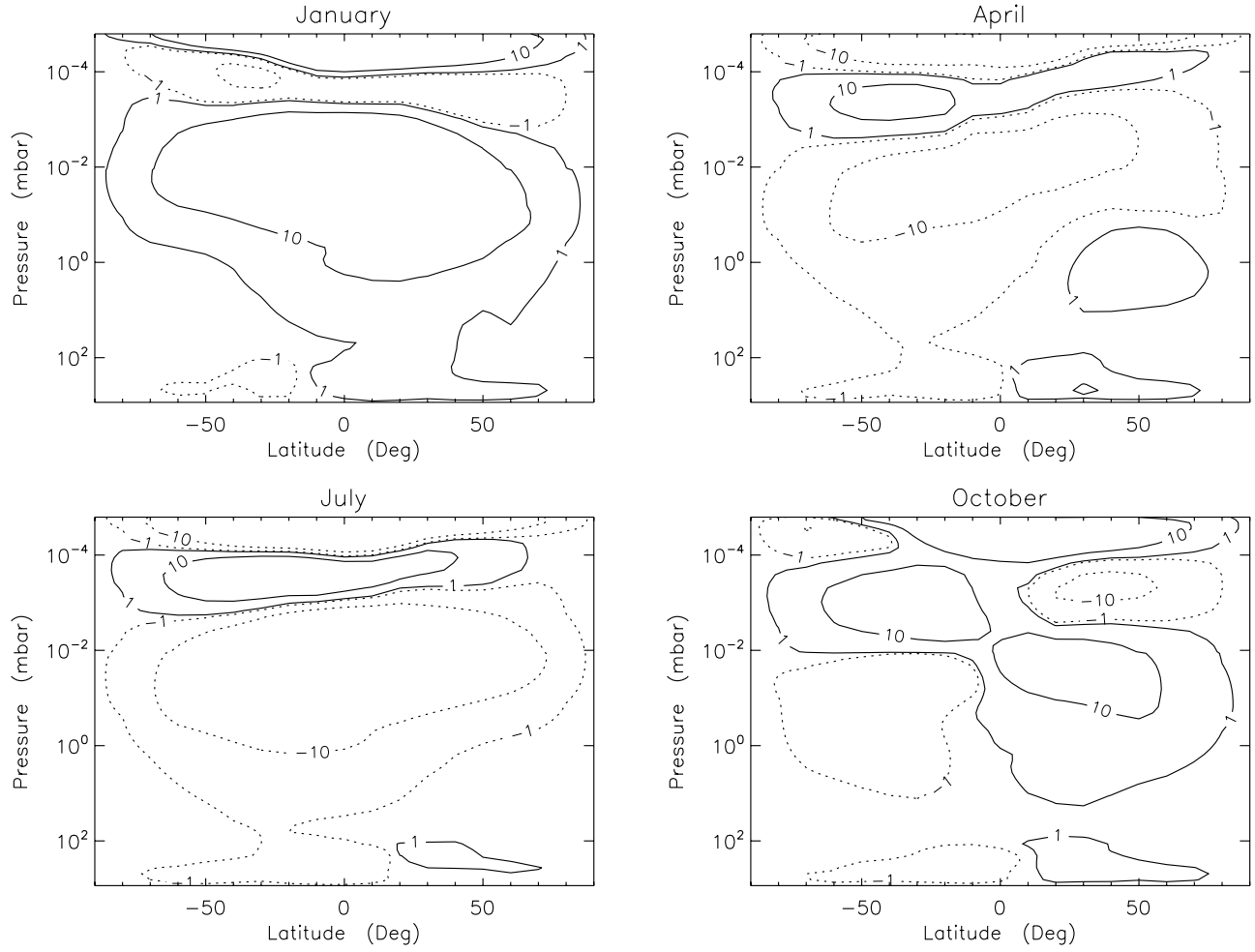

Figure 2. Contours of residual circulation derived from the WACCM simulations. The unit is 10^3 m^2 s^{-1}. Positive (negative) values denote clockwise (anticlockwise) circulation.

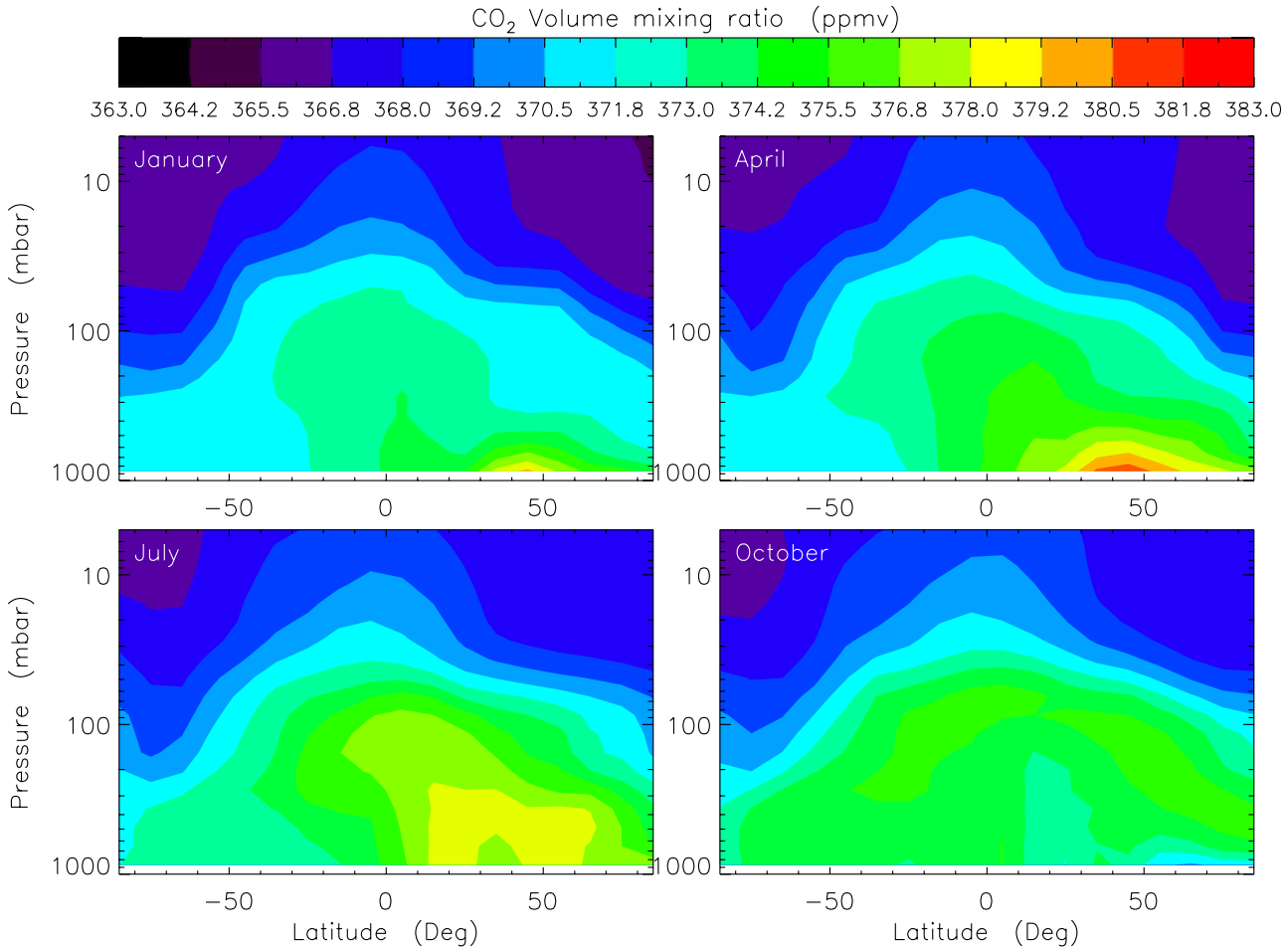

Figure 3. Latitude-pressure plots of modeled CO_2 mixing ratios for January, April, July, and October of 2003, using the residual circulation shown in Figure 2 (model B).

tion to 3.3 ± 0.1 PgC/a during 1980–1989 and to 3.2 ± 0.1 PgC/a over 1990–1999. The known sources and sinks of CO_2 are summarized in the 2001 IPCC report [*IPCC*, 2001].

[9] Nitrous oxide offers an example of using isotopic signatures to constrain trace gas sources and sinks [e.g., *Kim and Craig*, 1993; *Stein and Yung*, 2003]. The conceptual picture consists of three parts: (a) land biospheric sources of N_2O are strongly depleted in both ^{15}N and ^{18}O, compared with the mean tropospheric values; (b) oceanic sources are close to but slightly lighter than the mean tropospheric composition; and (c) there is a"back flux" of heavy N_2O from the stratosphere, where processes destructive of N_2O prefer the lighter isotopologues and isotopomers, to the troposphere. Thus the isotopic composition of tropospheric N_2O is a balance between biologically derived light N_2O and stratospheric heavy N_2O. Can a similar analysis be applied to CO_2?

[10] Unlike N_2O, which has no noticeable sink in the troposphere, CO_2 has significant gross carbon exchange between the atmosphere and the surface. (The insignificance of a nitrous oxide sink in the troposphere can be similarly inferred from the weak seasonality observed [*Liao et al.*, 2004; *Nevison et al.*, 2004]). The flux between the atmosphere and ocean and that between the atmosphere and land are 90 and 120 PgC/a, respectively, while the net flux to the ocean and land is only ~1.9 PgC/a. However, the net flux plays a fundamental role in determining the amount and isotopic composition of anthropogenic CO_2 that remains in the atmosphere, and since this flux is 2 orders of magnitude less than the gross carbon flux, the determination of sources and sinks of CO_2 is difficult.

[11] The isotopic composition of CO_2 in the atmosphere is an integrated signal of atmospheric and biogeochemical processes, and thus provides a tool for studying biogeochemical cycles involving CO_2 [e.g., *Ciais et al.*, 1997; *IPCC*, 2001]. To separate the different processes, several tracers must be used. For example, atmospheric $\delta^{13}C(CO_2)$ can differentiate the uptake fluxes of CO_2 by the land and ocean, while $\delta^{18}O(CO_2)$ provides a constraint on terrestrial gross primary production (GPP) [e.g., *Ciais et al.*, 1997; *IPCC*, 2001; *Cuntz et al.*, 2003a, 2003b] because the isotopic exchange reactions between CO_2 and two isotopically distinct water reservoirs (soil water and leaf water) are separable. In their troposphere-biosphere interactive model, for example, *Cuntz et al.* [2003a, 2003b] include four distinct sources of $\delta^{18}O(CO_2)$ to evaluate the budget of CO_2. Their model yields a northern hemispheric isoflux of −160 PgC/a which is balanced by an isoflux of +160‰ PgC/a in the southern hemisphere. In this paper, the input of heavy CO_2 from the stratosphere will be estimated and its

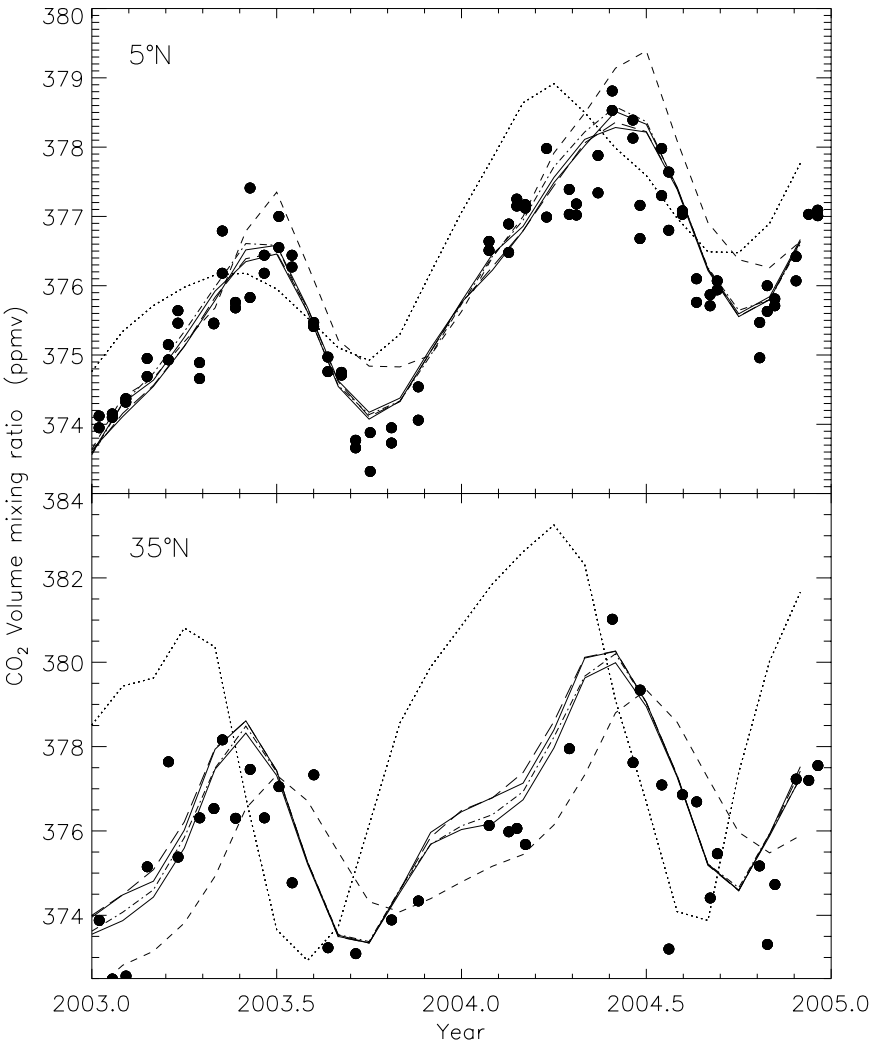

Figure 4. Aircraft observations between 9 km and 13 km (solid circles) [*Matsueda et al.*, 2002] and modeled CO_2 mixing ratios averaged over the layers between 9 km and 13 km in years 2003 and 2004. Models A-E are shown by solid, short-dashed, triple dot-dashed, long-dashed, and dash-dotted lines, respectively. For comparison, the surface CO_2 mixing ratios [*GLOBALVIEW-CO_2*, 2007] are shown by dotted lines.

impact on current CO_2 isotopic budgets examined. We note that middle atmospheric processes affecting the isotopic composition of CO_2 have not yet been included in current models [e.g., *Cuntz et al.*, 2003a, 2003b].

[12] In the atmosphere, the primary mechanism which modifies the isotopic composition of CO_2 is the exchange reaction with $O(^1D)$ in the stratosphere. This exchange process conserves the concentration of CO_2 but carries a very different isotopic signature from tropospheric/biospheric CO_2. In their two-box models, *Hoag et al.* [2005] investigate the contribution of stratospheric CO_2 to tropospheric/biospheric CO_2 based on the concept of mass-dependent and mass-independent fractionation processes, and find that the predicted $\Delta^{17}O(CO_2)$ is measurable with current instrumentation. Thus the isotopic composition of atmospheric CO_2 can, in principle, provide a new constraint on the gross carbon exchange between the biosphere and atmosphere in carbon cycle models [e.g., *Cuntz et al.*, 2003a, 2003b]. The uniqueness of $\Delta^{17}O$ is that it can be "reset" only by isotopic exchange reactions with water. This process has a long time constant, as compared with atmospheric transport timescales. For example, the isotopic exchange time of CO_2 with leaf water is ~2 years [*Ciais et al.*, 1997] while the transport time in the troposphere is on the order of months.

3. Mechanisms of CO_2 Isotopic Fractionation

[13] The isotopic composition of CO_2 is affected by that of $O(^1D)$ through the $CO_2 + O(^1D)$ exchange reaction. Ozone photolysis is the major source of $O(^1D)$ in the stratosphere, while O_2 Lyman α-driven photodissociation is important in the mesosphere [*Allen et al.*, 1981]. The former process produces a larger slope (~1.5–1.7) in three-isotope plots of oxygen in CO_2 than the latter (~0.3). This great difference can therefore provide a powerful tool for studying dynamics in the mesosphere (see below).

[14] We briefly summarize the basic features of the O_3 isotopic anomaly. The isotopic enrichment is primarily caused by the formation of O_3. As a consequence of finite

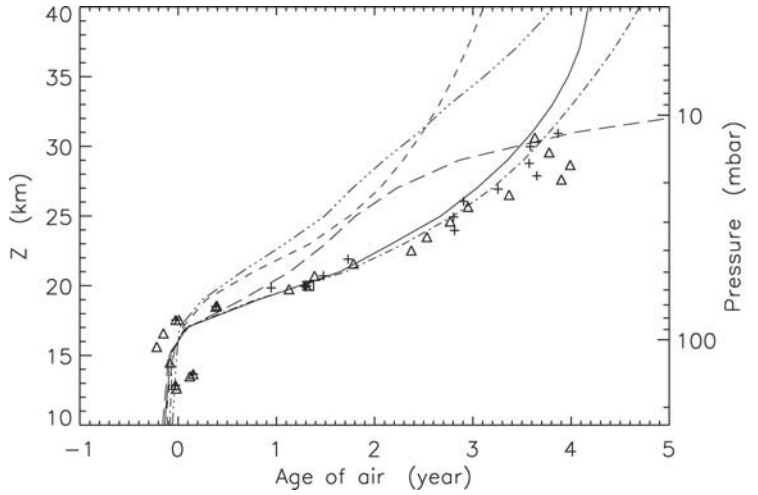

Figure 5. The vertical profile of the annually averaged age of air over 10°S to 10°N derived from the 2-D CTM simulations of CO_2. The lines have same meaning as in Figure 4. Also shown are the mean age calculated from balloon measurements of CO_2 (crosses) and SF_6 (triangles) taken during February and November 1997 at 7°S, and ER-2 aircraft measurements of CO_2 (asterisks) and SF_6 (squares) at 20 km averaged over 10°S–10°N during 1992–1997 [*Boering et al.*, 1996; *Elkins et al.*, 1996; *Ray et al.*, 1999; *Andrews et al.*, 2001].

lifetime of O_3 complex in the intermediate state, symmetric isotopomers in their intermediate states tend to have greater deviation from their statistical density of states, compared with asymmetric isotopomers. It is this deviation that produces $\delta^{49}O_3 \approx \delta^{50}O_3 \approx 100$ ‰, relative to atmospheric O_2. In addition, about 10% of the observed O_3 isotopic enrichment is due to photolytic processes. The photolysis effect provides an explanation for the observed altitude variation of the O_3 isotopic enrichments in the stratosphere. See *Liang et al.* [2006] for details. Following the same assumption as *Liang et al.* [2006, 2007] and *Liang and Yung* [2007], we only consider the terminal abstraction of ozone photolysis for the production of $O(^1D)$ atoms.

[15] Since the branch of O_2 photolysis to $O(^3P) + O(^1D)$ at Lyman α line is spin-forbidden, a strong wavelength-dependent isotopic fractionation in the quantum yield is expected and observed [*Lacoursière et al.*, 1999]. Previous quantum calculation and atmospheric modeling show that the isotopic fractionation at O_2 Lyman α photolysis is significant [*Liang et al.*, 2007].

[16] The atmospheric oxygen chemistry used here is that presented by *Liang et al.* [2006], while the O_2 Lyman α

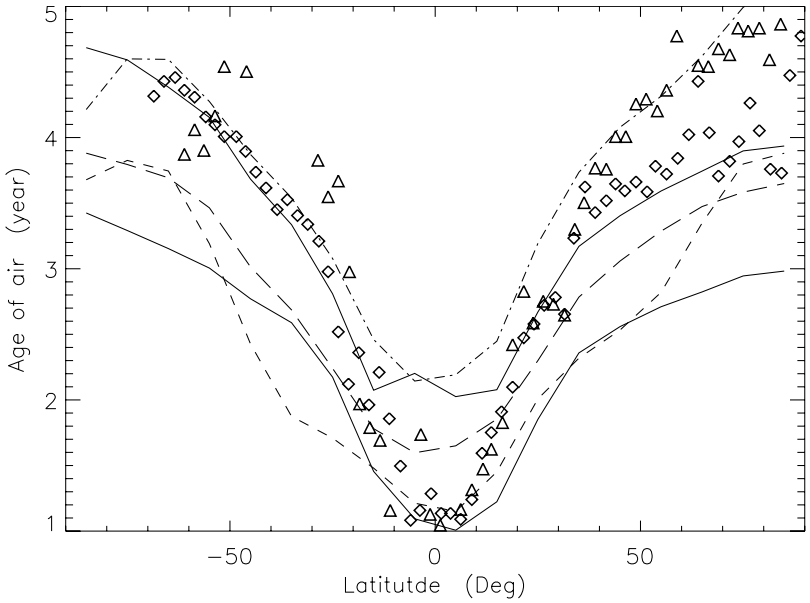

Figure 6. Modeled (lines) mean age of air versus observations (symbols) at ~20 km. The lines have same meaning as Figure 4. Diamonds and triangles are derived from CO_2 and SF_6, respectively, taken from *Boering et al.* [1996], *Elkins et al.* [1996], *Ray et al.* [1999], and *Andrews et al.*, 2001.

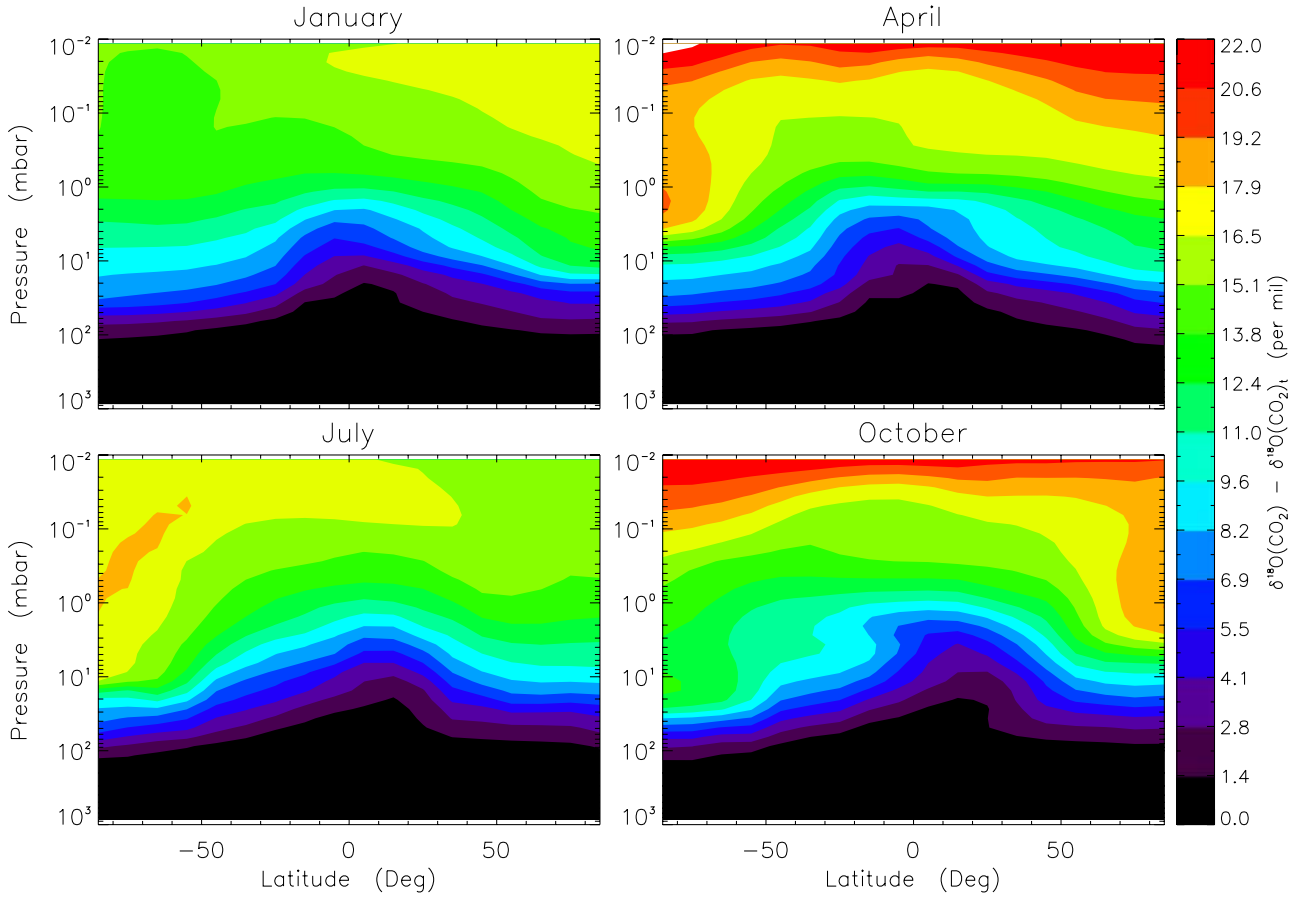

Figure 7. Modeled $\delta^{18}O(CO_2)$ for January, April, July, and October, using model A circulation. The mean tropospheric values ($\delta^{18}O(CO_2)_t$)have been subtracted.

photolytic cross sections and the specific five chemical reactions that fractionate the isotopic composition of CO_2 in the middle atmosphere, as shown below, are taken from *Liang et al.* [2007]:

$$\begin{array}{ll} {}^{16}O(^1D) + C^{16}O^{16}O \rightarrow C^{16}O^{16}O + {}^{16}O & k \\ {}^{17}O(^1D) + C^{16}O^{16}O \rightarrow C^{16}O^{17}O + {}^{16}O & k_1 = 2/3k(1+\xi_1) \\ {}^{16}O(^1D) + C^{16}O^{17}O \rightarrow C^{16}O^{16}O + {}^{17}O & k_2 = 1/3k(1+\xi_2) \\ {}^{18}O(^1D) + C^{16}O^{16}O \rightarrow C^{16}O^{18}O + {}^{16}O & k_3 = 2/3k(1+\xi_3) \\ {}^{16}O(^1D) + C^{16}O^{18}O \rightarrow C^{16}O^{16}O + {}^{18}O & k_4 = 1/3k(1+\xi_4), \end{array}$$

where O is either $O(^1D)$ or $O(^3P)$, k is the rate coefficient, and ξ_1–ξ_4 account for any deviation in the rate coefficients from simple counting statistics. Under these assumption, the isotopic composition of CO_2 in steady state can then be approximated by the following equations:

$$\begin{aligned} &\delta^{17}O(CO_2) - \delta^{17}O(CO_2)_t \\ &\quad \approx f_1\left[\xi_1 - \xi_2 + \delta^{17}O(^1D) - \delta^{17}O(CO_2)_t\right] \end{aligned} \tag{5}$$

$$\begin{aligned} &\delta^{18}O(CO_2) - \delta^{18}O(CO_2)_t \\ &\quad \approx f_2\left[\xi_3 - \xi_4 + \delta^{18}O(^1D) - \delta^{18}O(CO_2)_t\right], \end{aligned} \tag{6}$$

where $\delta^{17}O(CO_2)_t$ and $\delta^{18}O(CO_2)_t$ are tropospheric values. The symbols f_1 and f_2 represent modifications due to atmospheric transport; these two values are identical below the homopause. (The homopause divides the atmosphere into two regions: the homosphere and heterosphere. In the homosphere, the atmosphere is well-mixed. In the heterosphere, the density of a gas falls off with altitude at a rate dependent on molecular mass. In the Earth's atmosphere, the homopause is about 100 km above the surface.) Under current atmospheric conditions, the timescale of dynamical processes is shorter than that of the CO_2 isotopic exchange, resulting in a large modification of the isotopic enrichment of CO_2 that originates from exchange with $O(^1D)$. This is the main reason for the great difference between the isotopic composition of $O(^1D)$ (∼100‰) [*Liang et al.*, 2006; *Liang and Yung*, 2007] and that of CO_2 (∼10‰). The factor of 10 difference between $O(^1D)$ and CO_2 implies that $f_1 = f_2 \approx 0.1$, determined by the steady state assumption in equations (5) and (6). Note that the two equations are used only for the demonstration of the dynamical modification. The simulations solve the full algebraic equations in steady state to predict the isotopic composition of $O(^1D)$ and CO_2.

[17] The slope m in three-isotope plots of oxygen can thus be expressed by

$$m = \left[\delta^{17}O(CO_2) - \delta^{17}O(CO_2)_t\right] / \left[\delta^{18}O(CO_2) - \delta^{18}O(CO_2)_t\right]. \tag{7}$$

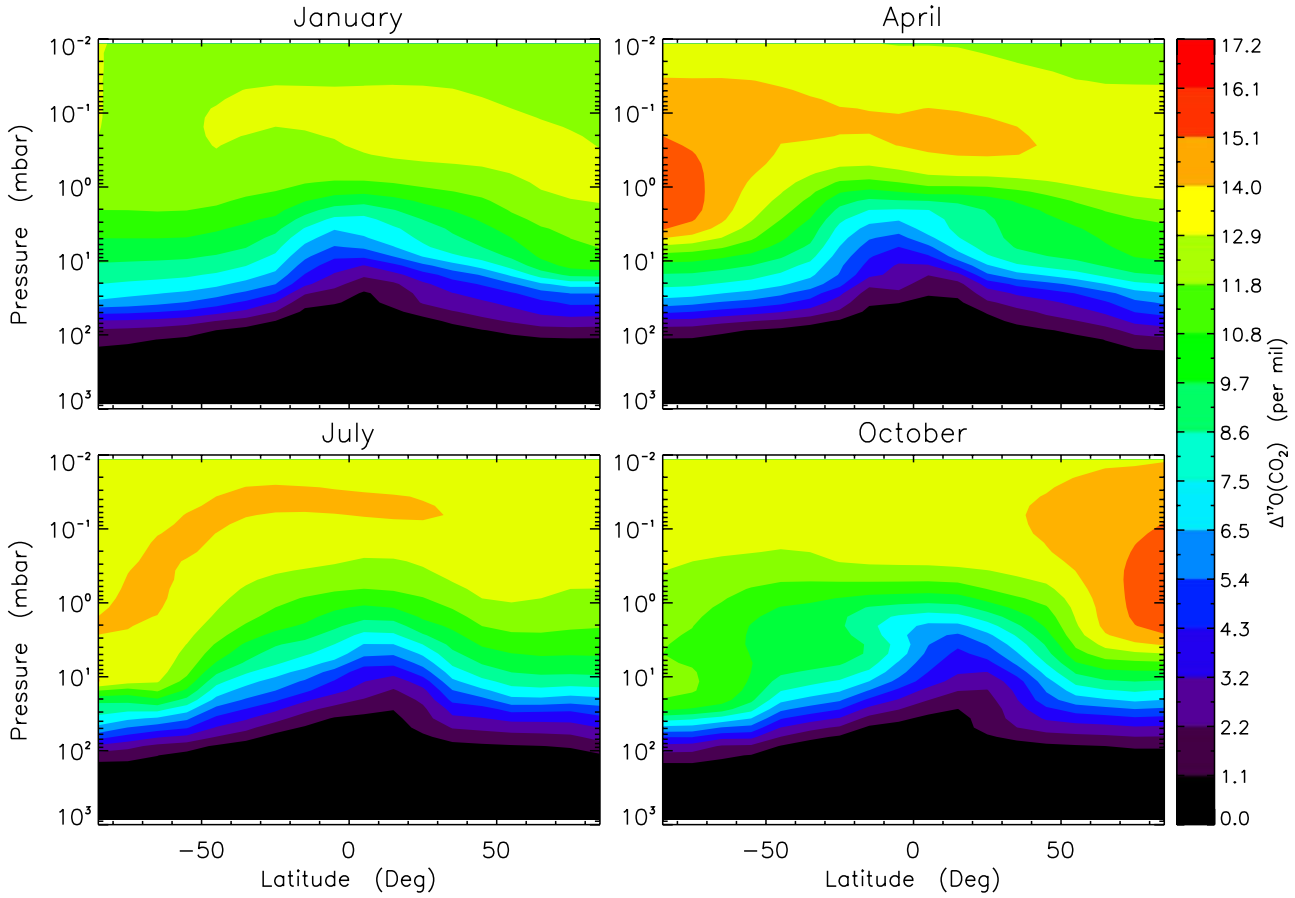

Figure 8. Same as Figure 7, for $\Delta^{17}O(CO_2)$.

[18] It is important to note that $\delta^{17}O(CO_2)$, $\delta^{18}O(CO_2)$, are a function of altitude and latitude, as is m (see below).

[19] As shown by *Liang et al.* [2007], our current (limited) understanding of the isotopic composition of CO_2 in the middle atmosphere can, in fact, be explained by a purely statistical accounting of the reaction probability, that is, $\xi_1 = \xi_2 = \xi_3 = \xi_4 = 0$; and so for simplicity we follow the same assumption in this paper. We do examine in section 6 the possibility that $\xi_1 - \xi_2 \neq \xi_3 - \xi_4$ can modify the slope m.

[20] As mentioned previously [*Liang et al.*, 2007], there are two major sources of isotopically anomalous $O(^1D)$. One is ozone photolysis, taking place mainly at ~15–70 km. The other is O_2 Lyman α photolysis for altitudes 70 km, and our model explicitly accounts for both sources of $O(^1D)$.

[21] Photolysis can also modify the isotopic composition of CO_2. Figure 1 presents the predicted fractionation factors of $C^{16}O^{18}O$ and $C^{16}O^{17}O$ using the method described elsewhere [*Yung and Miller*, 1997; *Miller and Yung*, 2000]. An overview of the photolytic fractionation factor is shown in the top panel, while the lower paper compares the results of a high spectral resolution calculation at ~185 nm as derived from the experimental results of *Bhattacharya et al.* [2000]. Though the photolysis at 185 nm causes the depletion of $C^{16}O^{18}O$, the overall photolytic processes enhances the heavy isotopologues (upper panel) because of the nearly featureless solar spectrum at wavelengths longer than 100 nm. Because of the low CO_2 photolysis rates compared with the reaction rates of CO_2 and $O(^1D)$, the effect of the photolysis of CO_2 produces a negligible (0.01‰) contribution to modifying its isotopic composition [see *Liang et al.*, 2007].

4. Data and Model Descriptions

[22] The Caltech/JPL 2-D chemistry transport model (2-D CTM) is used to simulate CO_2 isotopologue distributions in the atmosphere. A detailed description of the model can be found elsewhere [*Morgan et al.*, 2004]. Briefly, the model uses logarithmic pressure as the vertical coordinate, and has a 18 × 40 latitude-pressure grid extending from pole to pole and from the surface to about 80 km. For modeling studies in the mesosphere, we have included an option for extending the model to about 130 km (66 vertical layers). The transport is driven by three dynamical processes: residual circulations (ψ) and horizontal (K_{yy}) and vertical (K_{zz}) diffusivities. See *Morgan et al.* [2004] and *Jiang et al.* [2004] for details of the derivation of ψ and K_{yy}. The K_{zz} profiles are based on *Summers et al.* [1997], with some modifications in order to match the age of air measured in the stratosphere [see *Morgan et al.*, 2004].

[23] The time-varying observed surface CO_2 concentrations from 1975 to 2004 are taken from the National Oceanic and Atmospheric Administration (NOAA) Climate Monitoring and Diagnostics Laboratory (CMDL) [*Tans et*

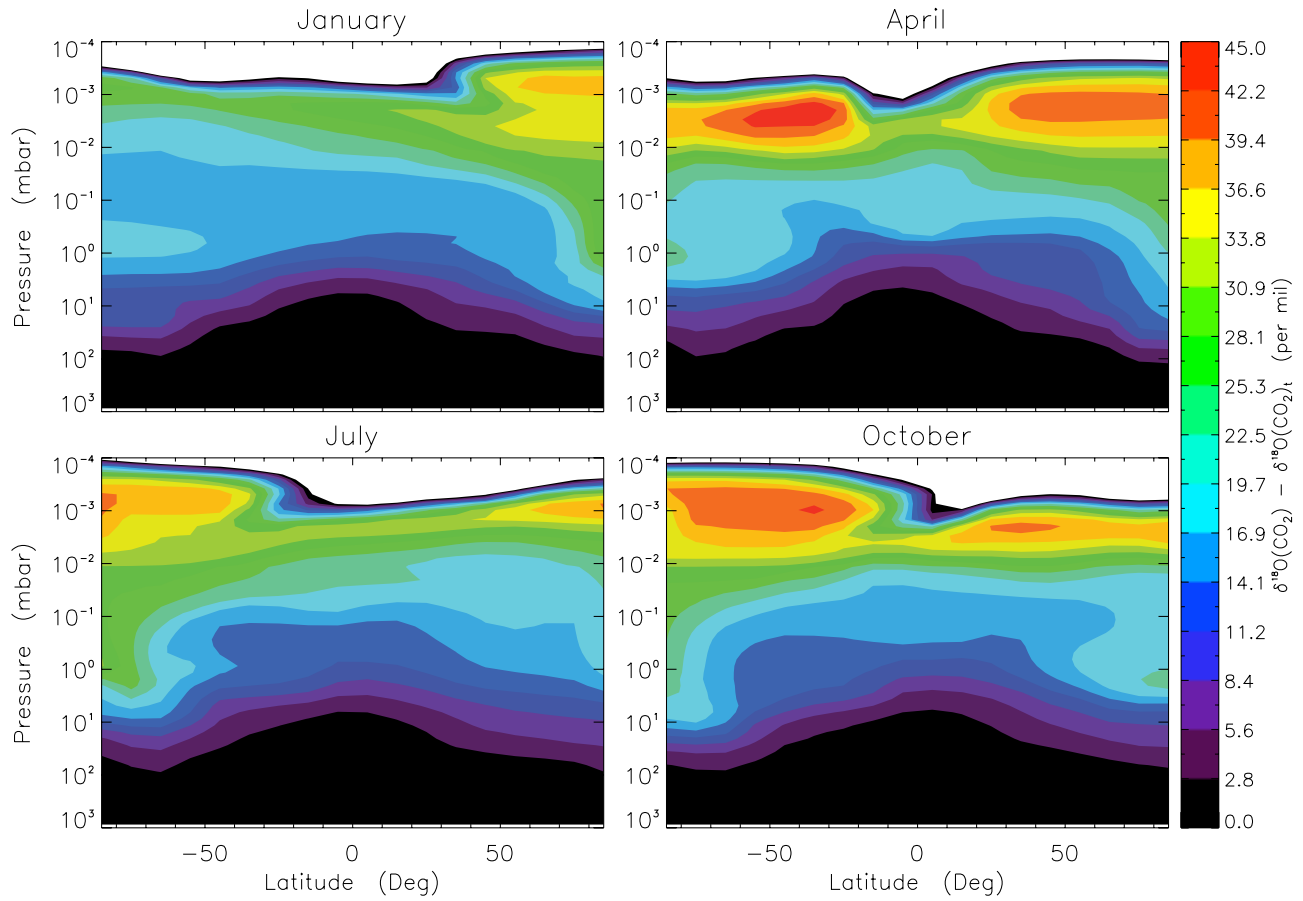

Figure 9. Same as Figure 7, for $\delta^{18}O(CO_2)$ computed by model B.

al., 1998; *GLOBALVIEW-CO_2, 2007*] and are used to define the lower boundary condition in our models. See *Shia et al.* [2006] for details. The isotopic composition of CO_2 is fixed at the lower boundary, with abundances set by the mean tropospheric values, i.e., $\delta^{17}O(CO_2)_t \approx 9$ and $\delta^{18}O(CO_2)_t \approx 17‰$ with respect to atmospheric O_2, or 21 and 41‰ relative to V-SMOW [*Thiemens et al.*, 1995]. Aircraft measurements of CO_2 mixing ratios at altitudes of ~8–13 km [*Matsueda et al.*, 2002] and age of air data [*Boering et al.*, 1996; *Elkins et al.*, 1996; *Hall et al.*, 1999; *Ray et al.*, 1999; *Andrews et al.*, 2001; *Waugh and Hall*, 2002] are used to validate the modeled atmospheric transport (see below).

[24] The transport (ψ, K_{yy}, and K_{zz}) of *Morgan et al.* [2004] is selected to be our reference case (model A), as it has been used to simulate the seasonality of upper tropospheric CO_2 [*Shia et al.*, 2006] and to the study of the sources of the oxygen isotopic anomaly in atmospheric N_2O [*Liang and Yung*, 2007]. Residual circulations (ψ) derived from the National Centers for Environmental Prediction-Department of Energy Reanalysis 2 (NCEP2) [*Kistler et al.*, 2001], European Centre for Medium-Range Weather Forecasts Reanalysis (ECMWF) [*Uppala et al.*, 2005], and Whole Atmosphere Community Climate Model (WACCM) outputs [*Sassi et al.*, 2002, 2004] are also included, in order to provide a model sensitivity analysis with respect to changes in circulation. The circulations from NCEP2 and ECMWF are good to ~40 km; ψ equals zero above the upper boundary of these two data sets. The upper boundary of WACCM is about 130 km, and can therefore provide a realistic circulation model of mesosphere-stratosphere exchange. Table 1 summarizes the sources of the transport fields used in this paper.

[25] Figure 2 presents the derived stream function from WACCM. The definition of the stream function follows that given by *Shia et al.* [1989]. This is distinct from the mass-weighted stream function and is presented here to better illustrate the altitude dependence of the residual circulation. The stream function is strong in the northern hemisphere in January, when the latitudinal temperature gradient and wave activities are significant. Air ascends from the equator, reaches the pole above the ~1 mbar altitude level, then descends into the polar region and eventually returns to the surface at midlatitudes. As a consequence, the age of air increases with latitude and reaches a maximum value at the winter pole [e.g., see *Hall et al.*, 1999]. During this time, CO_2 can react with $O(^1D)$, resulting in an enhancement of heavy CO_2 (see section 5). Similar behavior for ψ obtains in the summer (winter for southern hemisphere) with the roles of northern hemisphere and southern hemisphere reversed. The stream function becomes weaker in the spring and fall. Note that there is a transition at $\sim 10^{-4}$–10^{-2} mbar, where the stream function changes sign. The transition and inversion are caused by the breaking of gravity waves [e.g., see *Sassi et al.*, 2002]. This results in an inefficient air exchange between the upper and lower mesosphere, as previously

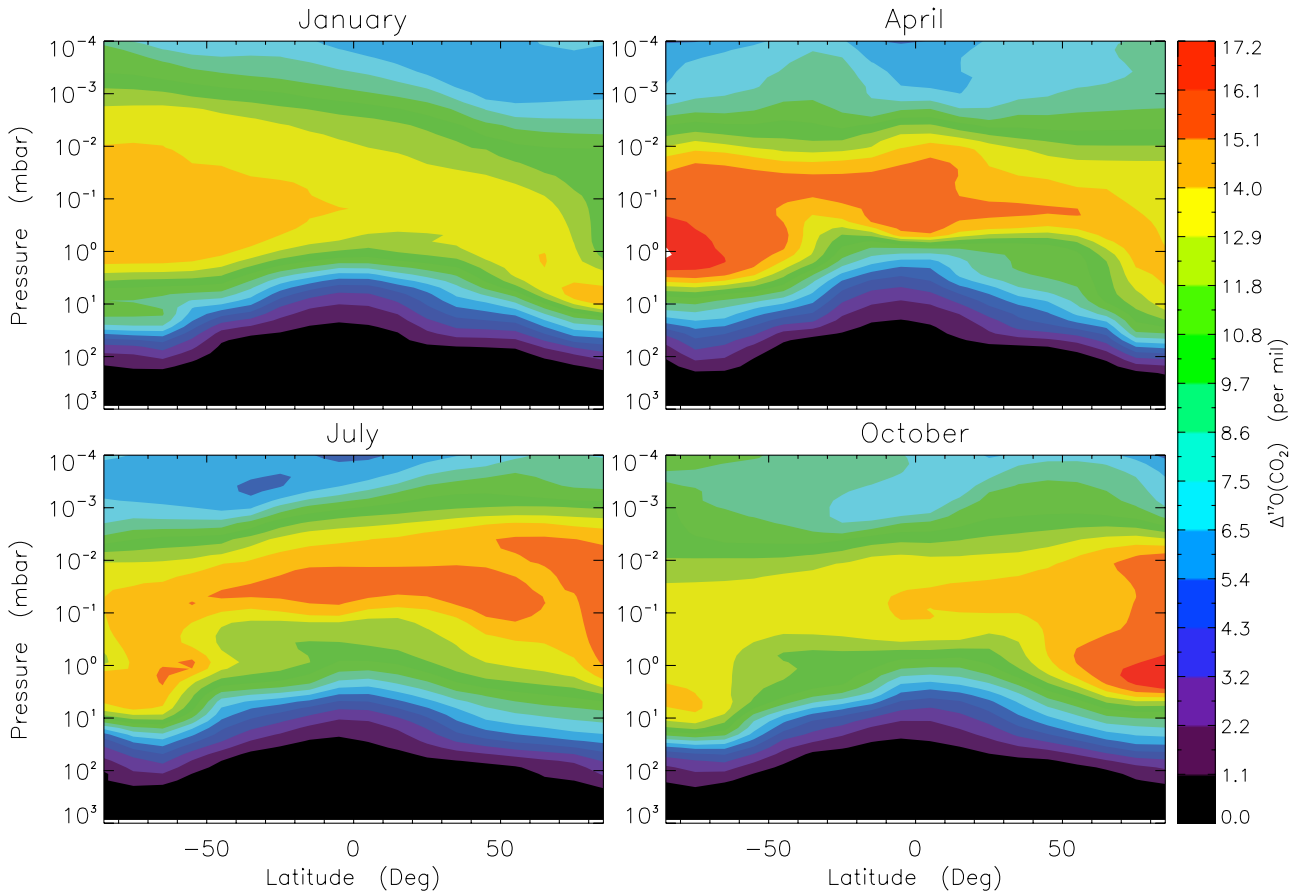

Figure 10. Same as Figure 9, for $\Delta^{17}O(CO_2)$.

noted in the form of a sharp decrease in K_{zz} above 80 km [e.g., *Allen et al.*, 1981; *Lindzen*, 1981; *Summers et al.*, 1997]. There is a strong seasonal cycle of CO_2 isotopic composition in this region (see section 5). The isotopic composition of CO_2 should therefore provide a powerful and unique tool for studying the dynamics in the high mesosphere, as more measurements become available.

[26] Shown in Figure 3 are the CO_2 distributions over four seasons, modeled with the WACCM ψ and the K_{yy} and K_{zz} (model B) of *Summers et al.* [1997]. Comparing with Figure 1 of *Shia et al.* [2006], the present model is more efficient in transporting material to higher altitudes. The discrepancy is mainly caused by K_{yy} and K_{zz}; the change of ψ has less impact to the CO_2 distribution (e.g., see models A versus E). A detailed comparison between the circulation fields follows.

[27] Two data sets provide constraints to the circulations: upper tropospheric CO_2 levels [*Matsueda et al.*, 2002] and the age of air in the stratosphere [*Boering et al.*, 1996; *Elkins et al.*, 1996; *Ray et al.*, 1999; *Andrews et al.*, 2001]. Figure 4 shows that the upper tropospheric CO_2 mixing ratios can be well reproduced by the models. For comparison, the surface CO_2 level is given by the dotted lines. Our model simulations are consistent with previous studies [*Shia et al.*, 2006] in which a 1–3 month lag in CO_2 seasonality is seen at ~10 km, as compared with surface CO_2. The lag is most likely the result of the time it takes for CO_2 to be transported from the surface to the tropical tropopause by the Hadley circulation, followed by stratosphere-troposphere exchange via the Brewer-Dobson circulation (see later discussion of the age of air in the upper troposphere and lower stratosphere). Differences in K_{yy} and K_{zz} also result in change to the seasonality of upper tropospheric CO_2 (e.g., see model B versus model A).

[28] Figures 5 and 6 show the vertical and latitudinal profiles of the age of air, respectively. Models A (solid lines) and E (dash-dotted lines) provide, in general, a better fit to the data. The other models are off by ~1 year, depending on altitude and latitude. Model B (short-dashed lines) shows shorter ages of air; while models C (triple dot-dashed lines) and D (long-dashed lines), with circulations derived from ECMWF and NCEP2, respectively, tend to have transport that is too fast.

5. Simulation Results

[29] The isotopic composition of $O(^1D)$ in the atmosphere is critical for modeling the oxygen anomaly in atmospheric CO_2. As described above, there are two major sources of $O(^1D)$ in the atmosphere: O_3 and O_2 photolysis. The former dominates in the stratosphere and provides sources of isotopically anomalous $O(^1D)$, mainly via the Hartley and Huggins bands of O_3. The latter source of anomalous $O(^1D)$ from O_2 photolysis arises mainly from solar Lyman α, and is significant only above ~70 km. See *Liang et al.* [2007] and *Liang and Yung* [2007] for details. The profiles of O_3

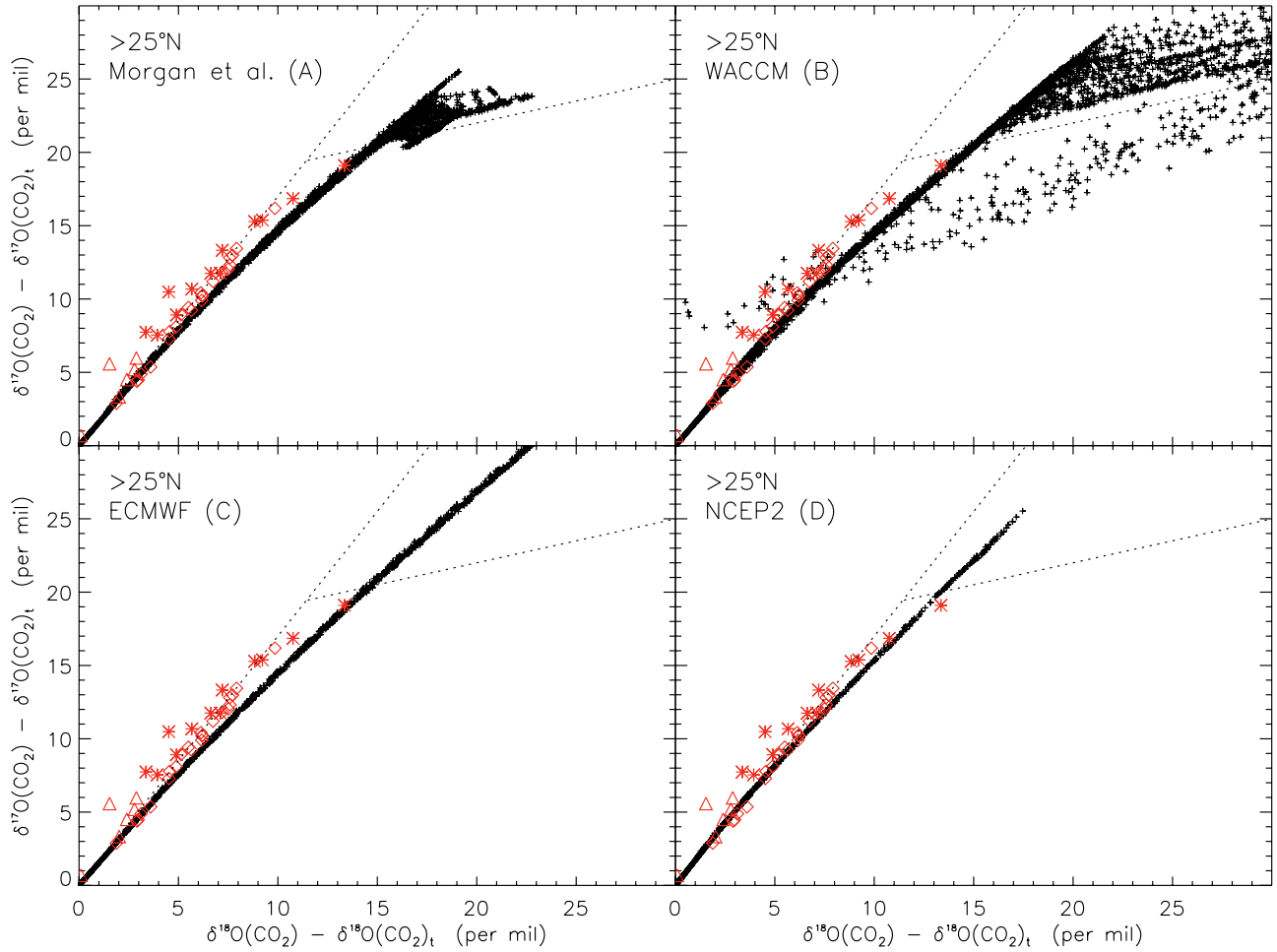

Figure 11. Three-isotope plot of oxygen in CO_2. The atmospheric measurements are from balloon measurements of *Lämmerzahl et al.* [2002] (diamonds) and *Alexander et al.* [2001] (triangles) and the rocket data reported by *Thiemens et al.* [1995] (asterisks). The crosses are model (models A-D, described in Table models) values at latitudes $\geq$25°N for all seasons. Two dotted lines draw m = 1.7 and 0.3. There is little difference between models A and E. Above ~90 km, molecular diffusion is important and m becomes ~0.5 (see model B).

and O(^{1}D) derived in this paper are the same as those by *Liang and Yung* [2007].

[30] The first stratospheric oxygen isotopic measurements of CO_2 were made by *Gamo et al.* [1989], who found that $\delta^{18}O(CO_2)$ increases with altitude, while measurements of the MIF of CO_2 (i.e., both $\delta^{17}O$ and $\delta^{18}O$) were pioneered by *Thiemens et al.* [1995], who took samples at 32.4°N and altitudes between ~29 and 61 km, in March and May of 1992. Subsequent stratospheric measurements were made at latitudes 43.7 and 67.9°N and altitudes ~20–33 km, in early summer through early winter [*Lämmerzahl et al.*, 2002]. Samples taken within the Arctic vortex (67.9°N) were reported by *Alexander et al.* [2001], who measured the $\delta^{17}O$ and $\delta^{18}O$ of CO_2 at altitudes between ~12 and 21 km on 11 February 1997. Later, *Boering et al.* [2004] measured the lower stratospheric isotopic composition of CO_2 from April through July of 1997 at altitudes between ~11 and 21 km and latitudes between ~48 and 90°N. Simulations from our 2-D CTMs will be compared with these measurements.

[31] Figures 7 and 8 present, respectively, the 2-D profiles of $\delta^{18}O(CO_2)$ and $\Delta^{17}O(CO_2)$ derived from model A. Generally speaking, the isotopic composition increases with altitude and latitude in the stratosphere, and is well correlated with the age of air described in Figures 5 and 6. In the mesosphere, the isotopic composition increases from the summer pole to the winter pole, consistent with the circulation shown in Figure 2. The correlation between the magnitude of the isotopic composition of CO_2 and age of air can be conceptually represented by equations (5) and (6) through the modification factor f that affects the δ values. The variations of $\delta^{18}O(CO_2)$ and $\Delta^{17}O(CO_2)$ are large in April and October when the circulation is weaker. In January, the strong stream function reduces the changes in the CO_2 isotopic composition that originate from the reaction with O(^{1}D). By comparison, transport is less efficient in April. Above 70 km, the isotopic composition of CO_2 is influenced primarily by O_2 photolysis at Lyman α.

[32] Figures 9 and 10 show the model results for $\delta^{18}O(CO_2)$ and $\Delta^{17}O(CO_2)$ from model B, which extends the model atmosphere up to 130 km. The O_2 Lyman α signature in this case cannot be transmitted efficiently to lower altitudes, due to the weak dynamical mixing between

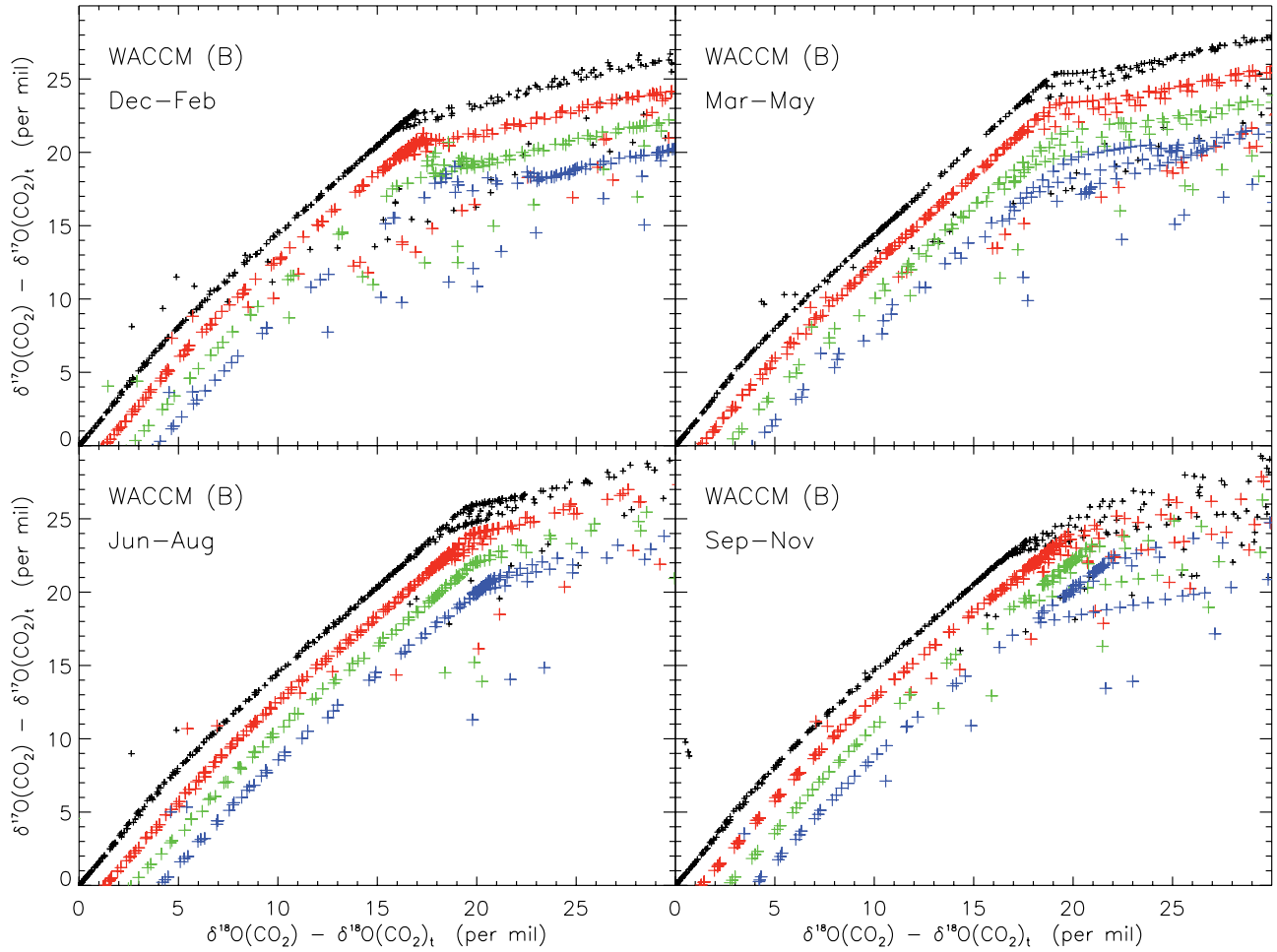

Figure 12. Same as for Figure 11 but with model B in four seasons. Model results at latitudes 25–50°N, 50–70°N, 70–80°N, and 80–90°N are shown by black, red, green, and blue symbols, respectively, with a vertical offset of −2 relative to the preceding one.

the upper and lower mesosphere (see also Figure 2). The abundances of heavy CO_2 are greatly enhanced in the region between $\sim 10^{-2}$ and 10^{-3} mbar. This is caused primarily by "closed" circulation cells in this region (see Figure 2), where the age of air is increased. Hence more CO_2 can react with $O(^1D)$. Notably, the strongest variations of the CO_2 isotopologues are in the spring and fall. The variation can be as high as 20‰, and provides an opportunity for verifying current models of dynamics in the mesosphere. Above $\sim 10^{-3}$ mbar (or 90 km, at the homopause), molecular diffusion dominates the transport and the isotopic fractionation of CO_2 becomes mass-dependent.

[33] Figure 11 shows three-isotope plots of oxygen in CO_2 derived from models A-D for all seasons at latitudes $\geq$25°N, along with atmospheric measurements [*Thiemens et al.*, 1995; *Lämmerzahl et al.*, 2002; *Alexander et al.*, 2001]. Because of possible mass-dependent fractionation artifacts (such as isotopic exchange with water) that affect both $\delta^{17}O(CO_2)$ and $\delta^{18}O(CO_2)$, but not $\Delta^{17}O(CO_2)$, the data of *Boering et al.* [2004] are not shown here. The linearly regressed slopes are insensitive to transport. The reason can be clearly seen in the equations (5)–(7). Transport below the homopause modifies both $\delta^{17}O(CO_2)$ and $\delta^{18}O(CO_2)$ by the same proportions [see also *Liang et al.*, 2007], and as the result, the slopes are controlled by two parameters: mean tropospheric δ values of CO_2 and isotopic composition of $O(^1D)$, which are kept unchanged between models. The figure also shows that there is little seasonal and latitudinal dependence on the slope m below $\sim$70 km (corresponding to $\delta^{18}O(CO_2) \approx 15‰$). This is consistent with the fact that the isotopic composition of O_3 (a source of $O(^1D)$) is only weakly dependent on temperature [*Liang et al.*, 2006, and references therein], that the spatiotemporal variation of stratospheric temperature is small, and that the CO_2 lifetime against the isotopic exchange with $O(^1D)$ is long [*Liang et al.*, 2007]. See also *Liang and Yung* [2007] for 2-D simulation of the isotopic composition of O_3. Above 70 km (model B), Lyman α photolysis of O_2 dominates and provides sources of $O(^1D)$ isotopically distinct from that of O_3 photolysis [*Liang et al.*, 2006, 2007; *Liang and Yung*, 2007]. Along with the strong seasonality in dynamics (Figure 2), the δ values are highly scattered above 70 km (see also Figure 9).

[34] Figure 12 shows an example of the latitudinal and seasonal variations of m, which can be used to divide the atmosphere into four regions: troposphere, stratosphere-lower mesosphere, upper mesosphere, and heterosphere. The first three constitute the homosphere. The δ values

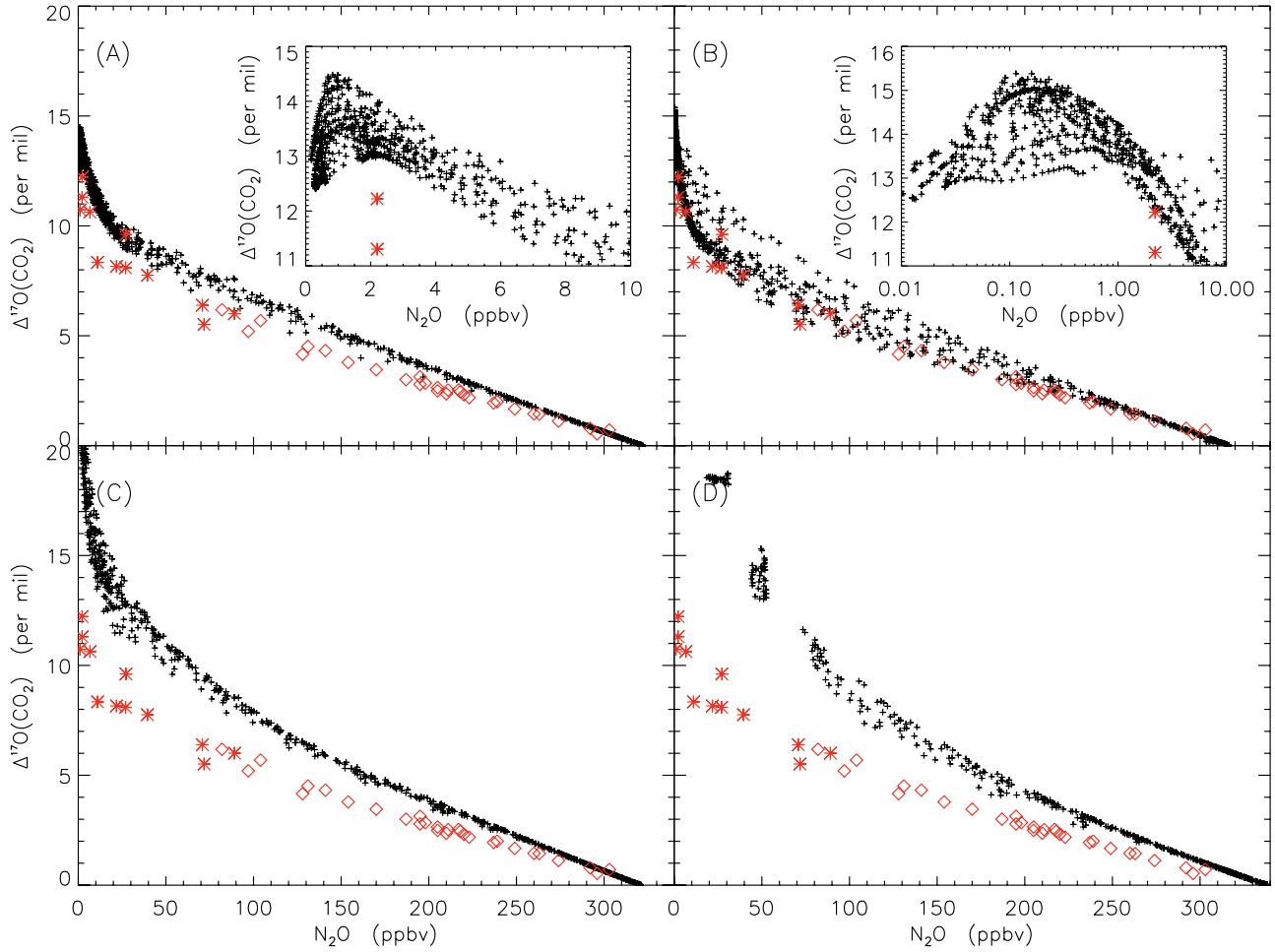

Figure 13. Plots of the value of $\Delta^{17}O(CO_2)$ versus nitrous oxide abundance for models A-D. Rocket (asterisks) and airborne (diamonds) data are taken from *Thiemens et al.* [1995] and *Boering et al.* [2004], respectively.

are uniform in the troposphere and increase rapidly in the middle atmosphere. In the stratosphere-lower mesosphere, m = 1.5. In the upper mesosphere, m = 0.3. The transition altitude lies near 70 km, corresponding to transition point A by *Liang et al.* [2007]. For comparison, the slopes of 1.7 from observations [*Lämmerzahl et al.*, 2002] and 0.3 [*Liang et al.*, 2007] are shown by dotted lines (Figure 11); the former slope represents stratospheric O_3 processes and the latter denotes mesospheric O_2 photolysis at Lyman α. The changes of m in the mesospheric measurements of CO_2 isotopologues [*Thiemens et al.*, 1995] suggest that the vertical mixing between upper and lower mesosphere is more efficient than that used in the current models. Future work with more realistic transport in this region is required, such as version 3 of WACCM model which is an interactive model of chemistry and dynamics [*Garcia et al.*, 2007]. In addition, it has been shown that the longitudinal variation is significant above the gravity wave breaking altitude (~70 km) [*Sassi et al.*, 2002], suggesting that 3-D modeling is needed for a quantitative comparison of predictions and measurements. Above ~90 km (the homopause), molecular diffusion process becomes important and m is 0.5 (see model B); this altitude is denoted as the transition point B by *Liang et al.* [2007].

[35] Figure 13 shows that the effects of dynamics and chemistry can clearly be separated. The $\Delta^{17}O(CO_2)$ values increase with altitude (decreasing N_2O mixing ratios) below ~70 km, but above 70 km, $\Delta^{17}O(CO_2)$ decreases with decreasing N_2O mixing ratio. The latter is caused by O_2 Lyman α photolysis that produces m less than 0.5, resulting in a turnover of $\Delta^{17}O(CO_2)$ at N_2O mixing ratios of 0.1–1 ppbv. The turnover of the N_2O mixing ratios is affected by atmospheric transport. The same feature has also been seen in 1-D models [*Liang et al.*, 2007]. The scatter of Δ values in Figure 13 is primarily caused by latitudinal variations of the age of air in the stratosphere (Figure 6). Figure 14 shows the Δ values as a function of latitude (separated by color) and season from model B, which confirms that the age of air determines the scatter in $\Delta^{17}O(CO_2)$ versus N_2O mixing ratio plots and that strong seasonality in circulations dominates the scatter in the upper mesosphere (see also Figure 10). There is a simple explanation for the scatter. Over the entire atmosphere, the CO_2 isotopic exchange time is longer than the transport time, but the lifetime of N_2O varies with altitude. In the lower stratosphere, the lifetime of N_2O against photolysis is longer than the transport time, resulting in less scatter in the region. Higher in the upper stratosphere and mesosphere, the N_2O lifetime decreases

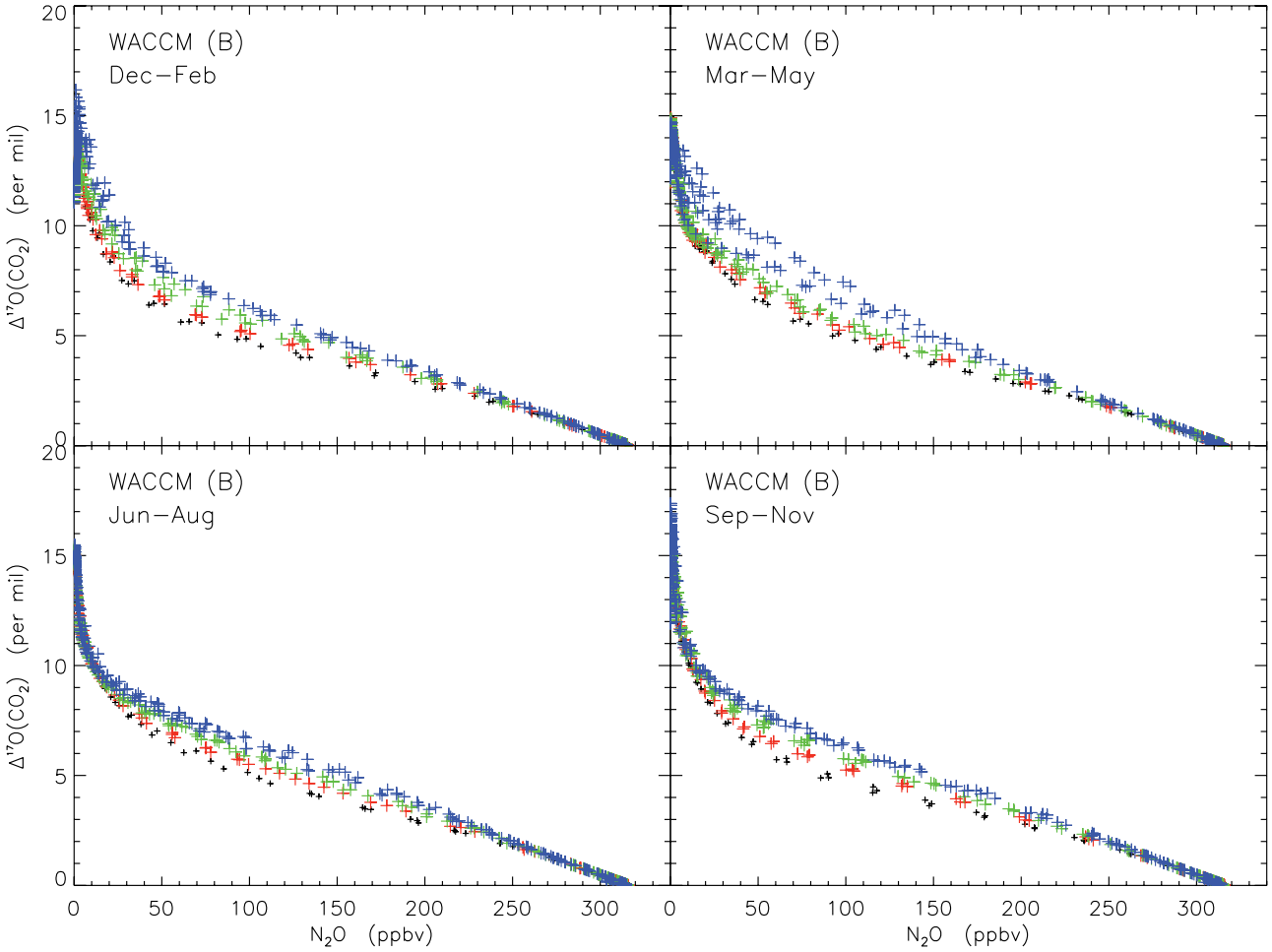

Figure 14. Same as for Figure 11 but with model B in four seasons. Model results at latitudes 25–30°N, 30–40°N, 40–60°N, and 60–90°N are shown by black, red, green, and blue symbols, respectively.

and the scatter becomes significant. Until the transport time is shorter than the N_2O lifetime, the scatter remains small.

6. Discussion and Summary

[36] We have demonstrated that the observed $\delta^{17}O$ and $\delta^{18}O$ values of CO_2 can be explained by the isotopic exchange between $O(^1D)$ and CO_2 in the middle atmosphere, although the modeled slope $m = 1.5$ is less than the observed slope of 1.7. The difference may well be resolved by a better understanding of dynamical and photochemical processes in the atmosphere (see below). In the stratosphere, the major source of $O(^1D)$ is O_3 photolysis in the Hartley-Huggins bands. Higher in the upper mesosphere, the source of heavy $O(^1D)$ is dominated by O_2 photolysis at Lyman α. The isotopic signature of $O(^1D)$ produced in the upper mesosphere is distinct from that in the stratosphere. The former gives $m \approx 0.3$, while the latter results in $m \approx 1.7$. Dynamical mixing between the upper ($m = 0.3$) and lower ($m = 1.7$) mesosphere could result in the smaller observed slope of 1.2 in mesospheric samples [*Thiemens et al.*, 1995]. Incorporating these two sources of $O(^1D)$ into 2-D CTMs, the observed slope of ~1.2 is not reproduced, due to inefficient transport between the upper and lower mesosphere in current models. Similar inefficient estimates of transport are also observed for $\delta^{18}O$ in O_2 (Figure 15). The O_2 Lyman α photolysis causes the depletion of heavy O_2 in the regions above ~70. This signature can be transported to a lower latitude where the depletion was observed [*Thiemens et al.*, 1995]. In our current steady state model, we find that $\delta^{18}O = -0.3‰$ occurs at ~0.1 mbar (or 0.01 mbar without considering O_2 Lyman α-driven isotopic fractionation) in the spring at 32.4°N, where the depletion was observed. The corresponding altitude of 0.1 mbar in April is 65 km, higher than the observed depletion altitudes of 53.3 and 59.5 km. Future work with refined dynamics in the mesosphere and 3-D models is required to validate the use of CO_2 isotopologues as tracers of the chemical and dynamical processes in the upper atmosphere.

[37] In the stratosphere and lower mesosphere, the modeled m is 1.5, less than the observed 1.72 ± 0.22 (2σ) at high latitudes [*Lämmerzahl et al.*, 2002] and 2.06 ± 1.16 (2σ) from the Arctic vortex [*Alexander et al.*, 2001]. Two sources of bias could result in this discrepancy. Our current model can explain the observed altitude variation of $\delta^{49}O_3$ and $\delta^{50}O_3$, but overestimates their absolute values [*Liang et al.*, 2006; *Liang and Yung*, 2007]. For example, assuming $\delta^{18}O(^1D) = 100‰$, the "effective" $\delta^{17}O(^1D) = 133.5‰$ for $m = 1.5$ (equation (7) is used). As shown by *Liang et al.* [2006] and *Liang and Yung* [2007], we overestimate $\delta^{50}O_3$

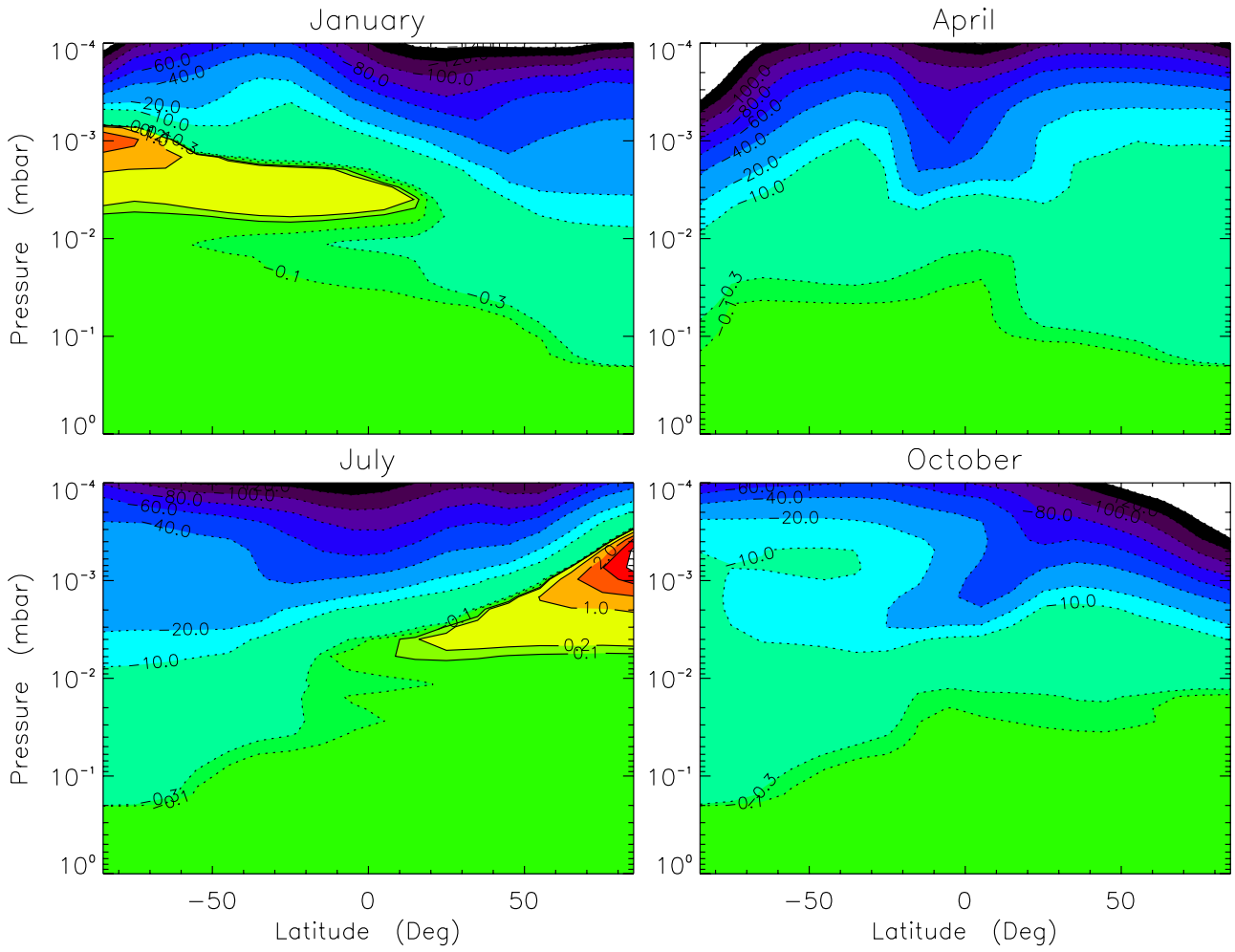

Figure 15. Modeled $\delta^{18}O$ of O_2 for January, April, July, and October, from model B. The contours are for $\delta^{18}O$ levels of −170 (black), −140, −110, −80, −60, −40, −20, −10, −0.3, −0.1, 0.1, 0.2, 1, 2, 3, and 4 (red) ‰. The predicted positive values are caused by photochemistry of O_2 [see also *Liang et al.*, 2007] and dynamics [*Summers et al.*, 1997].

by ∼20‰. The same overestimation is also applied to $\delta^{18}O(^1D)$. If $\delta^{18}O(^1D)$ is decreased by 20 (15)‰, the corrected m = 1.8 (1.7).

[38] Atmospheric transport could also modify m in an air parcel as it travels through the atmosphere. As we have discussed previously [*Liang et al.*, 2007], the isotopic composition of $O(^1D)$ from O_3 photolysis is a function of altitude, and therefore the age of air. The resulting m, in the absence of transport, ranges from 1.3 to 3.0. We note that as long as transport is reasonable, the resulting slopes are insensitive to the selection of transport (see above).

[39] Can mechanisms other than $CO_2 + O(^1D)$ contribute to the MIF of CO_2? The CO + OH reaction [*Röckmann et al.*, 1998], as a source of CO_2, can modify the isotopic composition of carbon dioxide in the troposphere; the reaction enhances $\delta^{18}(CO_2)$ by ∼10‰ and $\Delta^{17}(CO_2)$ by ∼2–5‰, depending on pressure. However, to have a significant effect on the atmospheric CO_2 or m, the required reaction rate of CO + OH must be at least as high as that of $CO_2 + O(^1D)$, a value that is unreasonable. It is also possible [*Mebel et al.*, 2004] that the $CO_2 + O(^1D)$ exchange processes are isotopically dependent, i.e., $\xi_1 \neq \xi_2 \neq \xi_3 \neq \xi_4 \neq 0$; for example, for $\xi_1 - \xi_2 \approx -15$‰ (from the over estimated $\delta O(^1D)$ noted above), the required $\xi_3 - \xi_4 \approx -9$‰ in order to explain m = 1.7.

[40] The 2-D CTM models also explain the lower δ values of CO_2 observed by *Thiemens et al.* [1995] at ∼30°N at altitudes similar to those sampled by *Lämmerzahl et al.* [2002] but at higher latitudes. The lower values are caused by younger air parcels entering the stratosphere, confirming previous suggestions [e.g., *Yung et al.*, 1997; *Liang et al.*, 2007].

[41] The $\delta^{17}O$ and $\delta^{18}O$ values of CO_2 have great utility as a tracer of atmospheric dynamics and chemistry from the surface to the mesosphere. For example, the isotopically exchanged CO_2 in the middle atmosphere carries a long-lived isotopic signature that is distinct from that in the troposphere, and so has the potential to constrain biogeochemical cycles involving carbon dioxide, in particular those involving the biosphere [e.g., *Hoag et al.*, 2005]. More importantly, the close relationship between O_2 and CO_2 provides a tool to constrain biospheric productivity in the paleo-atmosphere [e.g., *Luz et al.*, 1999]; CO_2 alone is limited because of the oxygen isotopic exchange in the "quasi-liquid" layer on the surfaces of ice grains in firn [*Assonov et al.*, 2005]. All these applications require detailed knowledge of mass-dependent and mass-

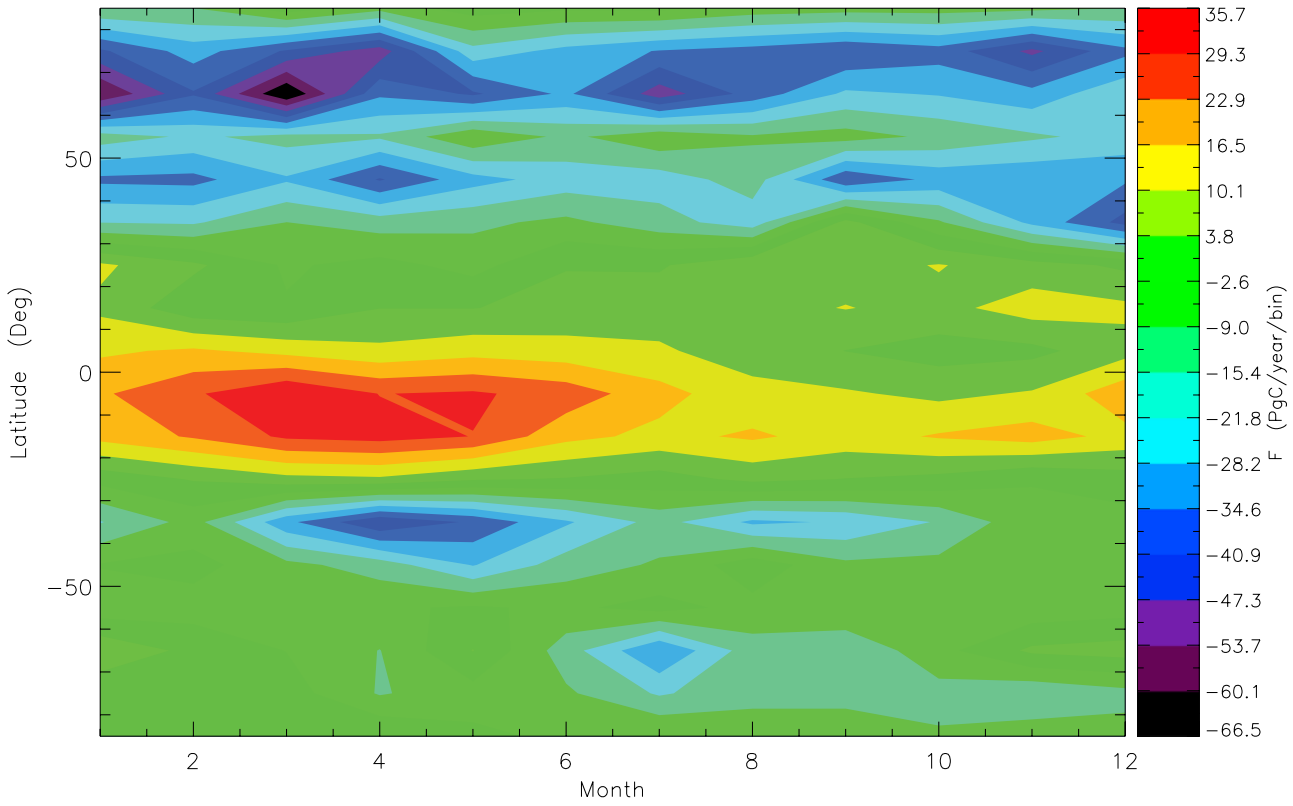

Figure 16. Seasonal cycle of the CO_2 flux across the tropopause in Pg of carbon per year per latitude bin of 10°. We follow the same definition of the tropopause (independent of season) as *Morgan et al.* [2004], in which the tropopause is approximately at 100 mbar between 30°S and 30°N, 200 mbar between 30° and 60°, and 300 mbar poleward of 60°. Negative and positive values represent downward and upward fluxes, respectively. The flux is taken from the year 2004 in model A.

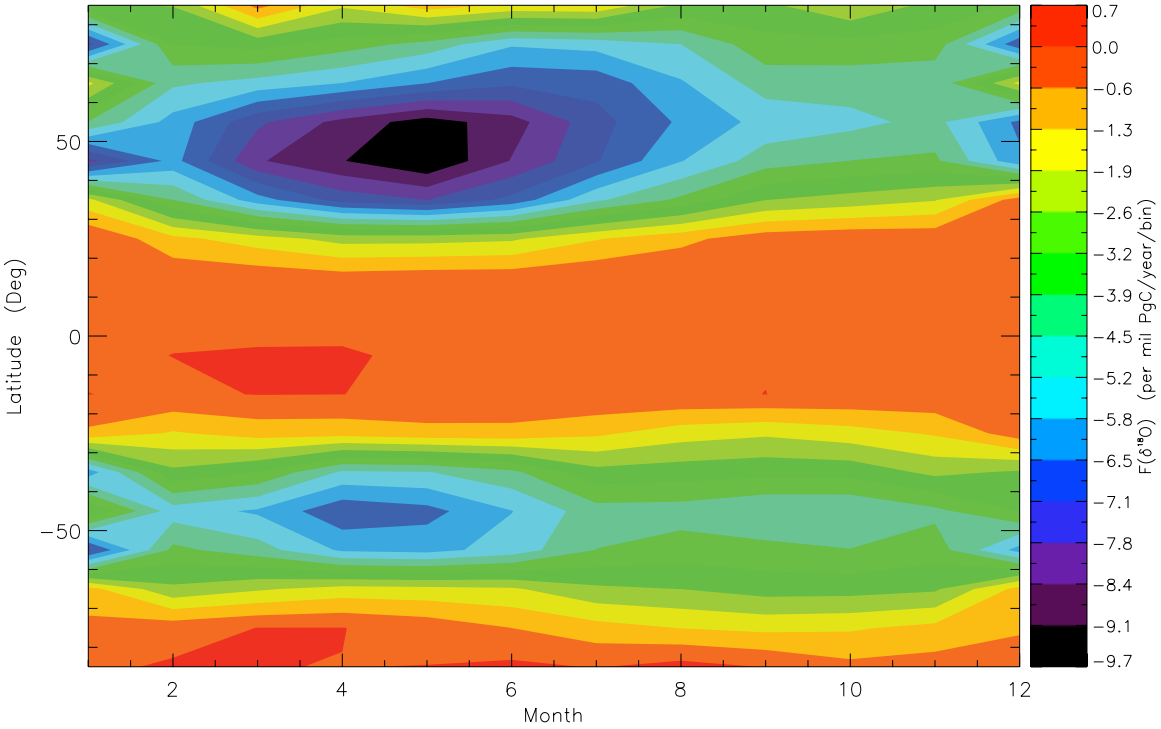

Figure 17. Seasonal cycle of the flux of $\delta^{18}O(CO_2)$ across the tropopause. The tropopause definition and model transport are the same as those of Figure 16.

Table 2. Cross-Tropopause Fluxes of $C^{16}O^{16}O$, $C^{16}O^{17}O$, and $C^{16}O^{18}O$[a]

	F	F(δ^{17}O)	F(δ^{18}O)	F(Δ^{17}O)
Model A	56.4	78.2	50.5	52.2
Model B	51.2	82.6	53.5	55.0
Model C	81.4	75.1	46.8	51.0
Model D	56.9	53.3	31.3	37.2
Model E	51.1	80.5	51.9	53.7
Averaged	59.4	73.9	46.8	49.8

[a]Downward fluxes (F) of CO_2 across the tropopause. Values of normal and isotopically substituted CO_2 are in PgC/a and ‰ PgC/a, respectively. F(Δ^{17}O) is defined as F(δ^{17}O) − 0.515 × F(δ^{18}O).

independent isotopic fractionation in O_2 and CO_2. Recent three-isotope measurements of O_2 in closed systems [*Luz and Barkan*, 2005] have shown that a nearly universal respiration curve can be used to extract highly precise Δ^{17}O values in O_2. Thus the MIF (in both O_2 and CO_2) at the surface reflects the magnitude of the anomalous signature generated in the middle atmosphere and the relative rates of mass transport through the biosphere.

[42] Figure 16 shows the cross-tropopause flux of CO_2. Figure 17 presents the seasonal variation of the isoflux of $\delta^{18}O(CO_2)$ across the tropopause, which arises because stratospheric processes enhance the abundance of $C^{16}O^{18}O$ relative to that in the troposphere. Negative values indicate that the flux is transported downward. The seasonal cycle shown here is different from that displayed at the surface (e.g., that dominated by biospheric processes, see *Cuntz et al.* [2003a]). Similar phenomena are demonstrated in Figure 4, in which there is a 1–3 month lag in CO_2 seasonality at ~10 km relative to that at the surface as a result of the Brewer-Dobson circulation [*Shia et al.*, 2006]. The annually averaged fluxes of heavy CO_2 from the stratosphere, through stratosphere-troposphere exchange, are summarized in Table 2. The flux of $\Delta^{17}O(CO_2)$ obtained from this work supports that (42.9‰ PgC/a) used in previous studies [*Boering et al.*, 2004; *Hoag et al.*, 2005]. As modeled by *Cuntz et al.* [2003a, 2003b], the annual mean $C^{16}O^{18}O$ budget is −160‰ PgC/a in the northern hemisphere in the biosphere (balanced by the southern hemisphere). Our value is a factor of about four less than the annual mean biospheric budget of $C^{16}O^{18}O$ in each hemisphere. This suggests that future modeling should include stratospheric processes in order to provide a better constraint on the biogeochemical cycles of CO_2.

[43] **Acknowledgments.** This work was supported in part by an NSC grant 96-2628-M-001-018 to the Academia Sinica and an NSF grant ATM-0529268 to the California Institute of Technology. Special thanks are due Xun Jiang and Run-Lie Shia for assisting in the construction of stream functions needed for the 2-D models for invaluable discussions and John Eiler for pointing out the reference describing the CO_2-water isotopic exchange in firn.

References

Alexander, B., M. K. Vollmer, T. Jackson, R. F. Weiss, and M. H. Thiemens (2001), Stratospheric CO_2 isotopic anomalies and SF6 and CFC tracer concentrations in the Arctic polar vortex, *Geophys. Res. Lett.*, *28*, 4103–4106.

Allen, M., Y. L. Yung, and J. W. Waters (1981), Vertical transport and photochemistry in the terrestrial mesosphere and lower thermosphere (50-120 km), *J. Geophys. Res.*, *86*, 3617–3627.

Andrews, A. E., et al. (2001), Mean ages of stratospheric air derived from in situ observations of CO_2, CH_4, and N_2O, *J. Geophys. Res.*, *106*, 32,295–32,314.

Assonov, S. S., C. A. M. Brenninkmeijer, and P. Jockel (2005), The ^{18}O isotope exchange rate between firn air CO_2 and the firn matrix at three Antarctic sites, *J. Geophys. Res.*, *110*, D18310, doi:10.1029/2005JD005769.

Bhattacharya, S. K., J. Savarino, and M. H. Thiemens (2000), A new class of oxygen isotopic fractionation in photodissociation of carbon dioxide: Potential implications for atmospheres of Mars and Earth, *Geophys. Res. Lett.*, *27*, 1459–1462.

Blake, G. A., M. C. Liang, C. G. Morgan, and Y. L. Yung (2003), A Born-Oppenheimer photolysis model of N_2O fractionation, *Geophys. Res. Lett.*, *30*(12), 1656, doi:10.1029/2003GL016932.

Boering, K., A. Jackson, T. Hoag, K. J. Cole, A. S. Perri, M. Thiemens, and E. Atlas (2004), Observations of the anomalous oxygen isotopic composition of carbon dioxide in the lower stratosphere and the flux of the anomaly to the troposphere, *Geophys. Res. Lett.*, *31*, L03109, doi:10.1029/2003GL018451.

Boering, K. A., S. C. Wofsy, B. C. Daube, H. R. Schneider, M. Loewenstein, and J. R. Podolske (1996), Stratospheric mean ages and transport rates from observations of carbon dioxide and nitrous oxide, *Science*, *274*, 1340–1343.

Buchwitz, M., R. de Beek, S. Noel, J. P. Burrows, H. Bovensmann, H. Bremer, P. Bergamaschi, S. Korner, and M. Heimann (2005a), Carbon monoxide, methane and carbon dioxide columns retrieved from SCIAMACHY by WFM-DOAS: Year 2003 initial data set, *Atmos. Chem. Phys.*, *5*, 3313–3329.

Buchwitz, M., et al. (2005b), Atmospheric methane and carbon dioxide from SCIAMACHY satellite data: Initial comparison with chemistry and transport models, *Atmos. Chem. Phys.*, *5*, 941–962.

Chakraborty, S., and S. K. Bhattacharya (2003), Oxygen isotopic fractionation during UV and visible light photodissociation of ozone, *J. Chem. Phys.*, *118*, 2164–2172.

Ciais, P., et al. (1997), A three-dimensional synthesis study of $\delta^{18}O$ in atmospheric CO_2: 1. Surface fluxes, *J. Geophys. Res.*, *102*, 5857–5872.

Cole, A. S., and K. A. Boering (2006), Mass-dependent and non-mass-dependent isotope effects in ozone photolysis: Resolving theory and experiments, *J. Chem. Phys.*, *125*, 184301.

Crisp, D., et al. (2004), The orbiting carbon observatory (OCO) mission, *Adv. Space Res.*, *34*, 700–709.

Cuntz, M., P. Ciais, G. Hoffmann, and W. Knorr (2003a), A comprehensive global three-dimensional model of $\delta^{18}O$ in atmospheric CO_2: 1. Validation of surface processes, *J. Geophys. Res.*, *108*(D17), 4527, doi:10.1029/2002JD003153

Cuntz, M., P. Ciais, G. Hoffmann, C. E. Allison, R. J. Francey, W. Knorr, P. P. Tans, J. W. C. White, and I. Levin (2003b), A comprehensive global three-dimensional model of $\delta^{18}O$ in atmospheric CO_2: 2. Mapping the atmospheric signal, *J. Geophys. Res.*, *108*(D17)4528, doi:10.1029/2002JD003154.

Elkins, J. W., et al. (1996), Airborne gas chromatograph for in situ measurements of long-lived species in the upper troposphere and lower stratosphere, *Geophys. Res. Lett.*, *23*, 347–350.

Gamo, T., M. Tsutsumi, H. Sakai, T. Nakazawa, M. Tanaka, H. Honda, H. Kubo, and T. Itoh (1989), Carbon and oxygen isotopic ratios of carbon dioxide of a stratospheric profile over Japan, *Tellus, Ser. B*, *41*, 127–133.

Gao, Y. Q., and R. A. Marcus (2001), Strange and unconventional isotope effects in ozone formation, *Science*, *293*, 259–263.

Garcia, R. R., D. R. Marsh, D. E. Kinnison, B. A. Boville, and F. Sassi (2007), Simulation of secular trends in the middle atmosphere, 1950–2003, *J. Geophys. Res.*, *112*, D09301, doi:10.1029/2006JD007485.

GLOBALVIEW-CO_2 (2007), *Cooperative Atmospheric Data Integration Project: Carbon Dioxide* [CD-ROM], NOAA ESRL, Boulder, Colo. (Available at ftp.cmdl.noaa.gov)

Hall, T. M., D. W. Waugh, K. A. Boering, and R. A. Plumb (1999), Evaluation of transport in stratospheric models, *J. Geophys. Res.*, *104*, 18,815–18,839.

Hitchcock, A. P., C. E. Brion, and M. J. Vanderwiel (1980), Absolute oscillator-strengths for valence-shell ionic photofragmentation of N_2O and CO_2 (8–75 ev), *Chem. Phys.*, *45*, 461–478.

Hoag, K. J., C. J. Still, I. Y. Fung, and K. A. Boering (2005), Triple oxygen isotope composition of tropospheric carbon dioxide as a tracer of terrestrial gross carbon fluxes, *Geophys. Res. Lett.*, *32*, L02802, doi:10.1029/2004GL021011.

IPCC (2001), Climate Change: The Scientific Basis, edited by J. T. Houghton, et al., Cambridge Univ. Press, New York.

Jiang, X., C. D. Camp, R. Shia, D. Noone, C. Walker, and Y. L. Yung (2004), Quasi-biennial oscillation and quasi-biennial oscillation-annual beat in the tropical total column ozone: A two-dimensional model simulation, *J. Geophys. Res.*, *109*, D16305, doi:10.1029/2003JD004377.

Kim, K. R., and H. Craig (1993), ^{15}N and ^{18}O characteristics of nitrous oxide - A global perspective, *Science*, *262*, 1855–1857.

Kistler, R., et al. (2001), The NCEP-NCAR 50-year reanalysis: Monthly means CD-ROM and documentation, *Bull. Am. Meteorol. Soc.*, *82*, 247–267.

Kuang, Z. M., J. Margolis, G. Toon, D. Crisp, and Y. Yung (2002), Spaceborne measurements of atmospheric CO_2 by high-resolution NIR spectrometry of reflected sunlight: An introductory study, *Geophys. Res. Lett.*, *29*(15), 1716, doi:10.1029/2001GL014298.

Lacoursière, J., S. A. Meyer, G. W. Faris, T. G. Slanger, B. R. Lewis, and S. T. Gibson (1999), The O (^{1}D) yield from O_2 photodissociation near H Lyman-Alpha (121.6 nm), *J. Chem. Phys.*, *110*, 1949–1958.

Lämmerzahl, P., T. Röckmann, C. A. M. Brenninkmeijer, D. Krankowsky, and K. Mauersberger (2002), Oxygen isotope composition of stratospheric carbon dioxide, *Geophys. Res. Lett.*, *29*(12), 1582, doi:10.1029/2001GL014343.

Lawrence, G. M. (1972a), Photodissociation of CO_2 to produce CO ($a^3\Pi$), *J. Chem. Phys.*, *56*, 3435–3442.

Lawrence, G. M. (1972b), Production of O (^{1}S) from photodissociation of CO_2, *J. Chem. Phys.*, *57*, 5616–5617.

Lewis, B. R., and J. H. Carver (1983), Temperaturedependence of the carbon-dioxide photo-absorption cross-section between 1200 and 1970 Å, *J. Quant. Spectrosc. Radiat. Transfer*, *30*, 297–309.

Liang, M. C., and Y. L. Yung (2007), Sources of the oxygen isotopic anomaly in atmospheric N_2O, *J. Geophys. Res.*, *112*, D13307, doi:10.1029/2006JD007876.

Liang, M. C., G. A. Blake, and Y. L. Yung (2004), A semianalytic model for photo-induced isotopic fractionation in simple molecules, *J. Geophys. Res.*, *109*, D10308, doi:10.1029/2004JD004539.

Liang, M. C., F. W. Irion, J. D. Weibel, C. E. Miller, G. A. Blake, and Y. L. Yung (2006), Isotopic composition of stratospheric ozone, *J. Geophys. Res.*, *111*, D02302, doi:10.1029/2005JD006342.

Liang, M. C., G. A. Blake, B. R. Lewis, and Y. L. Yung (2007), Oxygen isotopic composition of carbon dioxide in the middle atmosphere, *Proc. Nat. Acad. Sci. U.S.A.*, *104*, 21–25.

Liao, T., C. D. Camp, and Y. L. Yung (2004), The seasonal cycle of N_2O, *Geophys. Res. Lett.*, *31*, L17108, doi:10.1029/2004GL020345.

Lindzen, R. S. (1981), Turbulence and stress owing to gravity-wave and tidal breakdown, *J. Geophys. Res.*, *86*, 9707–9714.

Luz, B., and E. Barkan (2005), The isotopic ratios $^{17}O/^{16}O$ and $^{18}O/^{16}O$ in molecular oxygen and their significance in biogeochemistry, *Geochim. Cosmochim. Acta*, *69*, 1099–1110.

Luz, B., E. Barkan, M. L. Bender, M. H. Thiemens, and K. A. Boering (1999), Triple-isotope composition of atmospheric oxygen as a tracer of biosphere productivity, *Nature*, *400*, 547–550.

Matsueda, H., H. Y. Inoue, and M. Ishii (2002), Aircraft observation of carbon dioxide at 8–13 km altitude over the western Pacific from 1993 to 1999, *Tellus, Ser. B*, *54*, 1–21. (http://gaw.kishou. go.jp/wdcgg.html)

Mauersberger, K. (1987), Ozone isotope measurements in the stratosphere, *Geophys. Res. Lett.*, *14*, 80–83.

Mauersberger, K., B. Erbacher, D. Krankowsky, J. Gunther, and R. Nickel (1999), Ozone isotope enrichment: Isotopomer-specific rate coefficients, *Science*, *283*, 370–372.

Mauersberger, K., P. Lämmerzahl, and D. Krankowsky (2001), Stratospheric ozone isotope enrichments-revisited, *Geophys. Res. Lett.*, *28*, 3155–3158.

Mebel, A. M., M. Hayashi, V. V. Kislov, and S. H. Lin (2004), Theoretical study of oxygen isotope exchange and quenching in the $O(^1D)+CO_2$ reaction, *J. Phys. Chem. A*, *108*(39), 7983–7994.

Miller, C. E., and Y. L. Yung (2000), Photo-induced isotopic fractionation, *J. Geophys. Res.*, *105*, 29,039–29,051.

Miller, C. E., R. M. Onorato, M. C. Liang, and Y. L. Yung (2005), Extraordinary isotopic fractionation in ozone photolysis, *Geophys. Res. Lett.*, *32*, L14814, doi:10.1029/2005GL023160.

Morgan, C. G., M. Allen, M. C. Liang, R. L. Shia, G. A. Blake, and Y. L. Yung (2004), Isotopic fractionation of nitrous oxide in the stratosphere: Comparison between model and observations, *J. Geophys. Res.*, *109*, D04305, doi:10.1029/2003JD003402.

Nakata, R. S., K. Watanabe, and F. M. Matsunaga (1965), Absorption and photoionization coefficient of CO_2 in the region 580–1670 Å, *Sci. Light Tokyo*, *14*, 54V71.

Nevison, C. D., D. E. Kinnison, and R. F. Weiss (2004), Stratospheric influences on the tropospheric seasonal cycles of nitrous oxide and chlorofluorocarbons, *Geophys. Res. Lett.*, *31*, L20103, doi:10.1029/2004GL020398.

Okabe, H. (1978), *Photochemistry of Small Molecules*, 431 pp., John Wiley, Hoboken, N. J.

Parkinson, W. H. (2003), Absolute absorption cross section measurements of CO_2 in the wavelength region 163–200 nm and the temperature dependence, *Chem. Phys.*, *290*, 251–256.

Ray, E. A., F. L. Moore, J. W. Elkins, G. S. Dutton, D. W. Fahey, H. Vomel, S. J. Oltmans, and K. H. Rosenlof (1999), Transport into the Northern Hemisphere lowermost stratosphere revealed by in situ tracer measurements, *J. Geophys. Res.*, *104*, 26,565–26,580.

Röckmann, T., C. A. M. Brenninkmeijer, G. Saueressig, P. Bergamaschi, J. N. Crowley, H. Fischer, and P. J. Crutzen (1998), Mass-independent oxygen isotope fractionation in atmospheric CO as a result of the reaction CO + OH, *Science*, *281*, 544–546.

Sassi, F., R. R. Garcia, B. A. Boville, and H. Liu (2002), On temperature inversions and the mesospheric surf zone, *J. Geophys. Res.*, *107*(D19), 4380, doi:10.1029/2001JD001525.

Sassi, F., D. Kinnison, B. A. Boville, R. R. Garcia, and R. Roble (2004), Effect of El Nino-Southern Oscillation on the dynamical, thermal, and chemical structure of the middle atmosphere, *J. Geophys. Res.*, *109*, D17108, doi:10.1029/2003JD004434.

Shemansky, D. E. (1972), CO_2 extinction coefficient 1700–3000 Å, *J. Chem. Phys.*, *56*, 1582–1587.

Shia, R. L., Y. L. Yung, M. Allen, R. W. Zurek, and D. Crisp (1989), Sensitivity study of advection and diffusion-Coefficients in a 2-dimensional stratospheric model using excess C-14 data, *J. Geophys. Res.*, *94*, 18,467–18,484.

Shia, R. L., M. C. Liang, C. E. Miller, and Y. L. Yung (2006), CO_2 in the upper troposphere: Influence of stratospheretroposphere exchange, *Geophys. Res. Lett.*, *33*, L14814, doi:10.1029/2006GL026141.

Slanger, T. G., and G. Black (1978), CO_2 photolysis revisited, *J. Chem. Phys.*, *68*, 1844–1849.

Stein, L. Y., and Y. L. Yung (2003), Production, isotopic composition, and atmospheric fate of biologically produced nitrous oxide, *Annu. Rev. Earth Planet. Sci.*, *31*, 329–356.

Summers, M. E., D. E. Siskind, J. T. Bacmeister, R. R. Conway, S. E. Zasadil, and D. F. Strobel (1997), Seasonal variation of middle atmospheric CH_4 and H_2O with a new chemical-dynamical model, *J. Geophys. Res.*, *102*, 3503–3526.

Tans, P. P., et al. (ed.) (1998), Carbon cycle, in *Chapter 2 in Climate Monitoring and Diagnostics Laboratory No. 24 Summary Report 1996–1997*, edited by D. J. Hoffmann et al., pp. 30–51, NOAA Environmental Research Laboratories, Boulder, Colo. (http://www.cmdl.noaa.gov/)

Thiemens, M. H. (1999), Atmosphere science - Mass-independent isotope effects in planetary atmospheres and the early solar system, *Science*, *283*, 341–345.

Thiemens, M. H. (2006), History and applications of mass-independent isotope effects, *Annu. Rev. Earth Planet. Sci.*, *34*, 217–262.

Thiemens, M. H., and J. E. Heidenreich (1983), The mass-independent fractionation of oxygen - A novel isotope effect and its possible cosmochemical implications, *Science*, *219*, 1073–1075.

Thiemens, M. H., T. Jackson, K. Mauersberger, B. Schueler, and J. Morton (1991), Oxygen isotope fractionation in stratospheric CO_2, *Geophys. Res. Lett.*, *18*, 669–672.

Thiemens, M. H., T. Jackson, E. C. Zipf, P. W. Erdman, and C. Vanegmond (1995), Carbon-dioxide and oxygen-isotope anomalies in the mesosphere and stratosphere, *Science*, *270*, 969–972.

Uppala, S. M., et al. (2005), The ERA-40 reanalysis, *Q. J. R. Meteorol. Soc.*, *131*, 2961–3012.

Waugh, D. W., and T. M. Hall (2002), Age of stratospheric air: Theory, observations, and models, *Rev. Geophys.*, *40*, Art No. 2231.(4) 1010, doi:10.1029/2000RG000101.

Yoshino, K., J. R. Esmond, Y. Sun, W. H. Parkinson, K. Ito, and T. Matsui (1996), Absorption cross section measurements of carbon dioxide in the wavelength region 118.7–175.5 nm and the temperature dependence, *J. Quant. Spectrosc. Radiat. Transfer*, *55*, 53–60.

Yung, Y. L., and C. E. Miller (1997), Isotopic fractionation of stratospheric nitrous oxide, *Science*, *278*, 1778–1780.

Yung, Y. L., W. B. DeMore, and J. P. Pinto (1991), Isotopic exchange between carbon-dioxide and ozone via O (^{1}D) in the stratosphere, *Geophys. Res. Lett.*, *18*, 13–16.

Yung, Y. L., A. Y. T. Lee, F. W. Irion, W. B. DeMore, and J. Wen (1997), Carbon dioxide in the atmosphere: Isotopic exchange with ozone and its use as a tracer in the aiddle atmosphere, *J. Geophys. Res.*, *102*, 10,857–10,866.

Zipf, E. C., and P. W. Erdman (1994), Studies of trace constituents in the upper stratosphere and mesosphere using cryogenic whole air sampling techniques, in *NASA UARP Research Summaries, 1992–1993: Report to the Congress and the Environmental Protection Agency*, *Tech. Rep. N-92-34099*, Natl. Aeron. Space Admin., Washington, DC, Jan.

G. A. Blake and Y. L. Yung, Division of Geological and Planetary Sciences and Division of Chemistry and Chemical Engineering, California Institute of Technology, MS150-21, 1200 E. California Blvd., Pasadena, CA 91125, USA. (gab@gps.caltech.edu; yly@gps.caltech.edu)

M.-C. Liang, Research Center for Environmental Changes, Academia Sinica, No. 128, Section 2, Academia Road, Nankang, Taipei 11529, Taiwan. (mcl@rcec.sinica.edu.tw)